

**FEEDBACK CONTROLLED HIGH FREQUENCY  
ELECTROCHEMICAL MICROMACHINING**

A Thesis

by

FATIH MERT OZKESKIN

Submitted to the Office of Graduate Studies of  
Texas A&M University  
in partial fulfillment of the requirements for the degree of

MASTER OF SCIENCE

August 2008

Major Subject: Mechanical Engineering

**FEEDBACK CONTROLLED HIGH FREQUENCY  
ELECTROCHEMICAL MICROMACHINING**

A Thesis

by

FATIH MERT OZKESKIN

Submitted to the Office of Graduate Studies of  
Texas A&M University  
in partial fulfillment of the requirements for the degree of

MASTER OF SCIENCE

Approved by:

Chair of Committee,	Wayne Nguyen P. Hung
Committee Members,	Won-jong Kim
	Xing Cheng
Head of Department,	Dennis L. O'Neal

August 2008

Major Subject: Mechanical Engineering

## ABSTRACT

Feedback Controlled High Frequency Electrochemical Micromachining. (August 2008)

Fatih Mert Ozkeskin, B.S., Sabanci University

Chair of Advisory Committee: Dr. Wayne Nguyen P. Hung

Microsystem and integrated circuitry components are mostly manufactured using semiconductor technologies. Fabrication using high strength metals, for demanding aerospace, mechanical, or biomedical applications, requires novel technologies which are different from those for silicon. A promising mass production method for micro/meso scale components is electrochemical micromachining.

The complex system, however, requires high precision mechanical fixtures and sophisticated instrumentation for proper process control. This study presents an electrochemical micromachining system with a closed-loop feedback control programmed using a conditional binary logic approach.

The closed-loop control is realized using electrical current as the dynamic feedback signal. The control system improves material removal rate by 250% through optimizing inter electrode gap and provides robust automation reducing machining variation by 88%. The new system evokes production of higher quality microcomponents. Workpiece damage is reduced by 97% and increased feature sharpness is observed.

To my mother, Hayrunnisa

## ACKNOWLEDGEMENTS

This material is based upon work performed under the National Science Foundation grant No. 0552885, and support from Agilent, TAMU-CONACyT, and Cideteq.

I would like to thank my thesis advisor, Dr. Wayne Hung, for his guidance and encouragement throughout the study. I was honored to be his student. I also thank Dr. Won-jong Kim and Dr. Xing Cheng for serving on my thesis committee.

I also want to thank Dr. Jay Porter for sharing his vast knowledge on virtual instrument development and programming with me. Thanks to my laboratory partner, Sriharsha Sundarram, for helping me every time I needed it.

Finally, thanks to my parents and my sister for their constant support and love.

## TABLE OF CONTENTS

	Page
ABSTRACT .....	iii
DEDICATION .....	iv
ACKNOWLEDGEMENTS .....	v
TABLE OF CONTENTS .....	vi
LIST OF FIGURES.....	viii
LIST OF TABLES .....	x
NOMENCLATURE.....	xi
1. INTRODUCTION.....	1
2. LITERATURE REVIEW.....	3
2.1. Electrolysis.....	3
2.2. Electrochemical Micromachining .....	4
2.2.1. System Parameters .....	8
2.2.1.1. Static Parameters .....	8
2.2.1.1.1. Electrolyte .....	8
2.2.1.1.2. Pulse Frequency .....	10
2.2.1.1.3. Tool Electrode .....	13
2.2.1.1.4. Workpiece Material.....	17
2.2.1.2. Dynamic Parameters.....	17
2.2.1.2.1. Inter Electrode Gap .....	18
2.2.1.2.2. Resistance.....	18
2.2.1.2.3. Current Density .....	19
2.2.2. Theory .....	20
2.2.2.1. Current Density and IEG Relation .....	20
2.2.2.2. Material Removal Rate.....	22
2.2.3. MicroECM Applications .....	23
2.2.3.1. Hole Drilling .....	23
2.2.3.2. Grinding .....	26
2.2.3.3. Feature Shaping.....	27
2.2.3.4. Deburring .....	29

	Page
2.2.4. System Control.....	30
2.2.4.1. Open-loop Control.....	30
2.2.4.2. Closed-loop Control .....	31
2.2.4.3. PID Control .....	35
3. SYSTEM PROCESS CONTROL.....	38
4. EXPERIMENTS .....	44
4.1. List of Equipment.....	44
4.1.1. Stepper Motors .....	45
4.1.2. Function Generator.....	45
4.1.3. Ammeter.....	46
4.1.4. Oscilloscope .....	46
4.1.5. Laser Displacement Sensor .....	46
4.1.6. Serial Interface Board.....	47
4.2. Setup .....	47
4.2.1. MicroECM Cell.....	47
4.3. Experiments.....	50
4.3.1. Open-loop Experiments.....	50
4.3.2. Closed-loop Experiments .....	51
4.3.2.1. Dimensional Study .....	51
4.3.2.2. Hysteresis Study .....	52
5. RESULTS AND DISCUSSION .....	54
5.1. Labview Programming.....	54
5.2. Effect of Frequency on the Hole Depth and Diameter.....	58
5.3. Hole Profile .....	61
5.4. System Hysteresis .....	64
5.5. Effect of Amplification .....	65
6. CONCLUSIONS & RECOMMENDATIONS .....	66
REFERENCES .....	68
APPENDIX A .....	72
APPENDIX B .....	76
APPENDIX C .....	98
VITA .....	99

## LIST OF FIGURES

FIGURE	Page
1 Electrolytic cell .....	4
2 MicroECM schematic view.....	6
3 Electrochemical shaping .....	7
4 Comparison of holes drilled into stainless steel in different electrolytes...	10
5 Feature profile evolution of a lateral etch on substrate .....	12
6 Array of holes drilled with different pulse parameters into stainless steel	13
7 Side effect .....	14
8 Longitudinal cross-section of drilled hole.....	15
9 Effect of tool electrode diameter on machining rate .....	15
10 Examples of microprobes.....	16
11 Variation of current density with equilibrium machining gap .....	20
12 Micro hole array .....	24
13 Hole close view .....	24
14 Canonical nozzle .....	25
15 Electrochemical grinding process .....	26
16 3D Cu structure and Cu tongue .....	27
17 Tool electrode and machined cavity.....	28
18 Freestanding microcantilever machined into stainless steel sheet .....	29
19 Machined piece with burrs and deburred piece.....	30



FIGURE	Page
20 Developed pulse micro-ECM system.....	33
21 Flow chart of gap control .....	34
22 Generic control system.....	35
23 Current and position feedback design .....	40
24 Flow chart of tool electrode position and velocity control.....	41
25 MicroECM cell with bi-slide actuator.....	48
26 Custom built microECM cell .....	48
27 Closed-loop microECM setup.....	50
28 Open-loop Labview program front panel.....	54
29 Closed-loop Labview program front panel .....	55
30 An example machining process.....	56
31 Effect of electrode gap on ECM current density.....	57
32 Effect of frequency on hole diameter .....	59
33 Effect of frequency on hole depth .....	60
34 Material removal rate with frequency .....	61
35 Cross sectional tool electrode and machined hole .....	62
36 MicroECM hole profile images.....	63
37 Hysteresis study.....	64
38 Effect of amplification .....	65

**LIST OF TABLES**

TABLE		Page
1	Parameters for dimensional study experiments.....	52
2	Parameters for hysteresis study experiments.....	53

**NOMENCLATURE**

$A$	Tool frontal end surface area
$E(t)$	Applied voltage
$e(t)$	Input error signal
$F$	Faraday constant
$f_r$	Feed rate
$g$	The tool-workpiece gap
$I$	Current
$i$	Dissolution current density
$i_0$	Exchange current density at equilibrium
$K_p$	Proportional gain
$K_i$	Integral gain
$K_d$	Derivative gain
$M$	Molecular weight of the dissolved material
$n$	Number of electrons
$R$	Material removal rate
$r$	Electrolyte resistivity
$R_g$	Gas constant
$t$	Time
$T_a$	Electrolyte temperature
$u(t)$	Output controller

$V$	Volume removed
$\beta$	Charge transfer coefficient
$\rho$	Material density
$\tau$	Pulse-on duration
$\varphi$	Over-potential

## 1. INTRODUCTION

Various methods for removing materials constitute the foundation in manufacturing systems and they have a leading role in the production of components in multi scale. Pioneer micro/nano fabrication methodologies appeared in integrated circuitry as silicon machining technology. The fabrication methodology of microsystems and integrated circuitry components was well-known and it became practically abundant (Rai-Coudhury 1997). The silicon micromachining technology was practiced in several applications for many years extending from microelectromechanical systems (MEMS) sensors and actuators (Jerman and Terry 1997) to biomedical uses (Santini, Cima and Langer 1999). The semiconducting properties of silicon make it popular in electronics, but lack of mechanical properties makes silicon vulnerable to many other applications that demands high stress and temperature. Micromachining of engineering alloys such as stainless steel, titanium or superalloys must be performed with alternative novel methods. An emerging non-conventional technology for micro/meso scale components is the electrochemical micromachining (microECM).

MicroECM has found its applications in a variety of industries: biomedical, aerospace, automotive, electronic, etc. Although the technique is advantageous in many applications, it has several drawbacks that needs to be addressed. A typical microECM is electrically and mechanically noisy and unstable due to vibrations and fluid motions. To improve the overall system performance, the driving mechanisms would need a robust controller to reduce environmental noise effects.

The objective of this study is to develop a closed-loop control system for enhancing the overall microECM process. The important factors of the software and hardware combinations are:

- Cost effective closed-loop system
- Reaching micron level precision
- Designing a user friendly interface

The scope is:

- Employing closed-loop control with electrical current feedback
- Utilize stainless steel (SS316L) as workpiece and tool electrodes
- Use sodium nitrate ( $\text{NaNO}_3$ ) electrolyte with constant concentration
- Control in 1 dimension (depth of electrode motion).

## 2. LITERATURE REVIEW

Electrochemical machining is a material removal technique that is based on anodic dissolution processes with workpiece being an anode and tool electrode being a cathode. Theoretical foundation comes from well established electrolysis phenomenon.

### 2.1. ELECTROLYSIS

Electrolysis is a method used to separate chemically bonded elements. The chemical reaction occurs when an electric voltage is applied across two electrodes submerged in a liquid. The ionized conductive liquid, called electrolyte, carries the dissolved atomic particles from one electrode to another. Electrolyte is a conventionally concentrated salt solution. The electrode where positive terminal of the power source is connected called the anode and the electrode where negative terminal of the power source is connected called the cathode. The system itself is called an electrolytic cell. A schematic of an electrolytic cell is illustrated in *Figure 1*. Anodic dissolutions are consequently followed by cathodic depositions. The positively charged ions travel towards the cathode and the negatively charged ions travel towards the anode. Electrolyte at its neutral form provides the balance between opposite charges. This balance provides a conservation of mass by equating mass of deposited material to mass of removed material. This is a bidirectional process where material deposition, called electroplating and material removal, called electropolishing is possible depending on the applied voltage polarity.

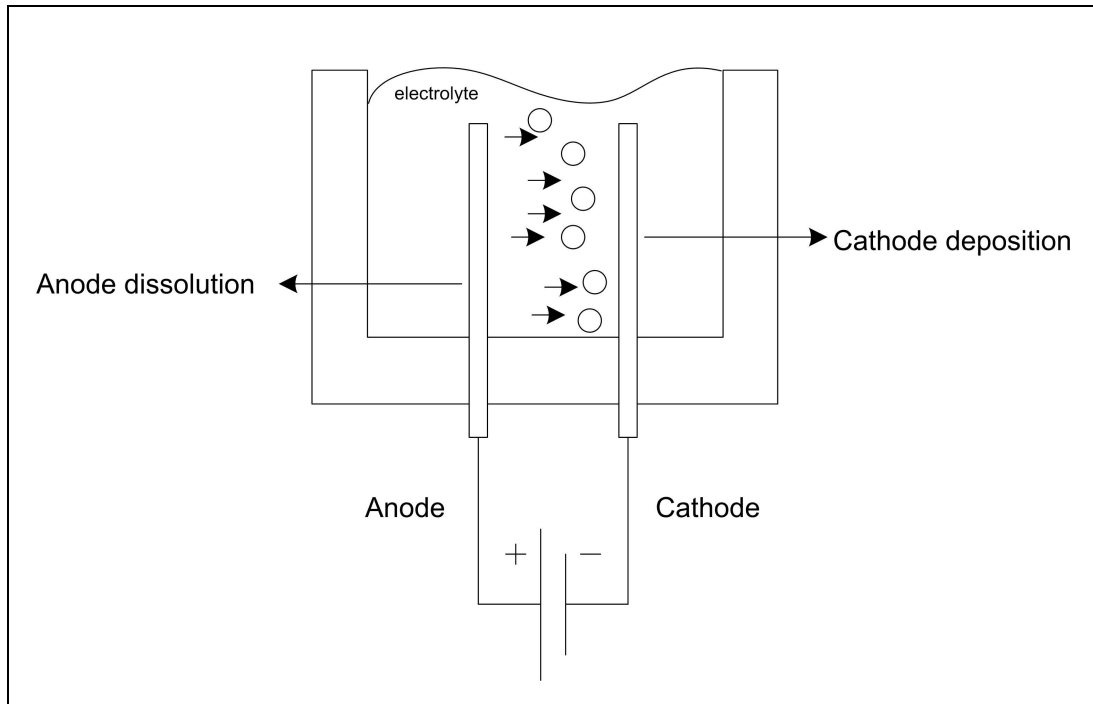


*Figure 1*  
**Electrolytic cell**

## **2.2. ELECTROCHEMICAL MICROMACHINING**

Electrochemical micromachining (microECM), is an evolved version of electrochemical polishing technique. In electrochemical polishing, the material removal is realized on a large surface, possibly all workpiece itself, exposed to material removal on a thin film formation, so that the roughness of a surface is reduced to have a shiny finish. Whereas, in microECM, the material removal is accomplished on a much more selectively concentrated area, using custom shaped tool electrodes. The tool electrode is used as a cathode and the workpiece is used as an anode where positive bias is applied.

For microECM to take place, the electrodes are brought into close proximity of generally sub-hundred micron, so that two oppositely charged electrodes can face on a



constrained area and start the reaction. Then, positive charged metal ions are removed from the workpiece. Oxidation reaction occurs at the anodic side since electrons are removed from the work piece, the reaction can be represented as,



where n is the valence of the work piece metal. The electrolyte collects the electrons resulting in a reduction which can be represented as,



Workpiece yields positive ions which react with the negative ions in the electrolyte solution. This forms hydroxides causing the dissolved metal precipitate in high rate. This cause an unwanted coating on machining region. With the reaction of contaminated products this could cause a formation of insulating layer which would decrease and even stop the reaction with time. If not contaminated, the same precipitation can grow a hill over the workpiece which can lead to short circuit between the two electrodes. To avoid this, the electrolyte is required to flush continuously over the machining zone. The electrolyte also carried away the heat and hydrogen bubbles formed due to chemical reaction. The electrolyte, since it carries the contaminated reactants, needs to be filtered. For this purpose, a filter is embedded in most electrolytic pump systems (Zhang et al. 2007). Electrolyte pump is widely used (Bhattacharyya, Munda and Malapati 2005). A schematic of a microECM system is given in *Figure 2*.

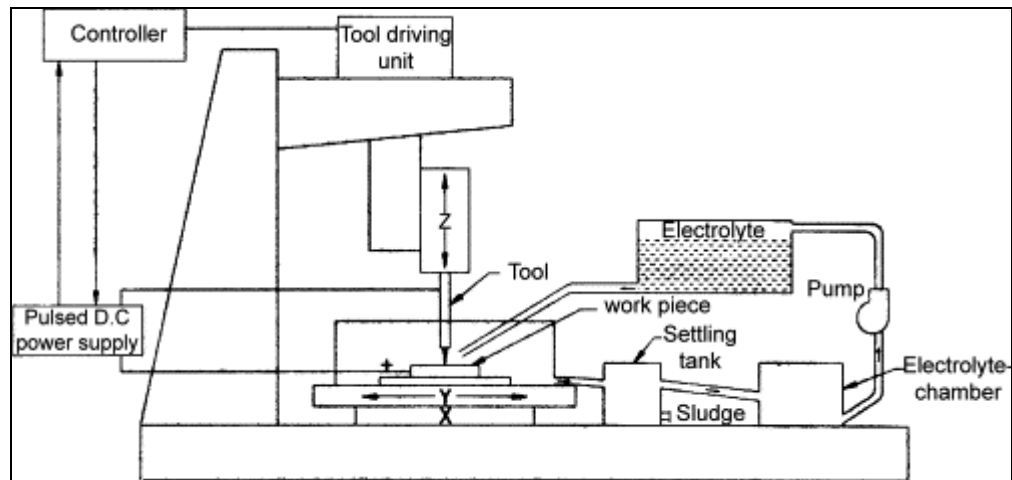


*Figure 2*  
**MicroECM schematic view (Bhattacharyya, Munda and Malapati 2005)**

The shape of the tool electrode, after machining, is projected on the surface of the work electrode. The tool electrode forms a negative shape of work electrode after successful machining. Tool electrodes are custom shaped to be able to form negative of the tool electrode on the workpiece. (Davydov, Volgin and Lyubimov 2004). Shaped tool electrode is transitionally advanced over the workpiece, making a shape projection. Therefore, tool shape defines the workpiece shape. Unshaped tool electrode, for instance a cylindrical tubular electrode also can be coordinated on a specific contour to provide same shape as in conventional milling processes. The latter approach is much more time consuming given the fact that the tool electrode travels a longer contour distance. An example is depicted in *Figure 3*.

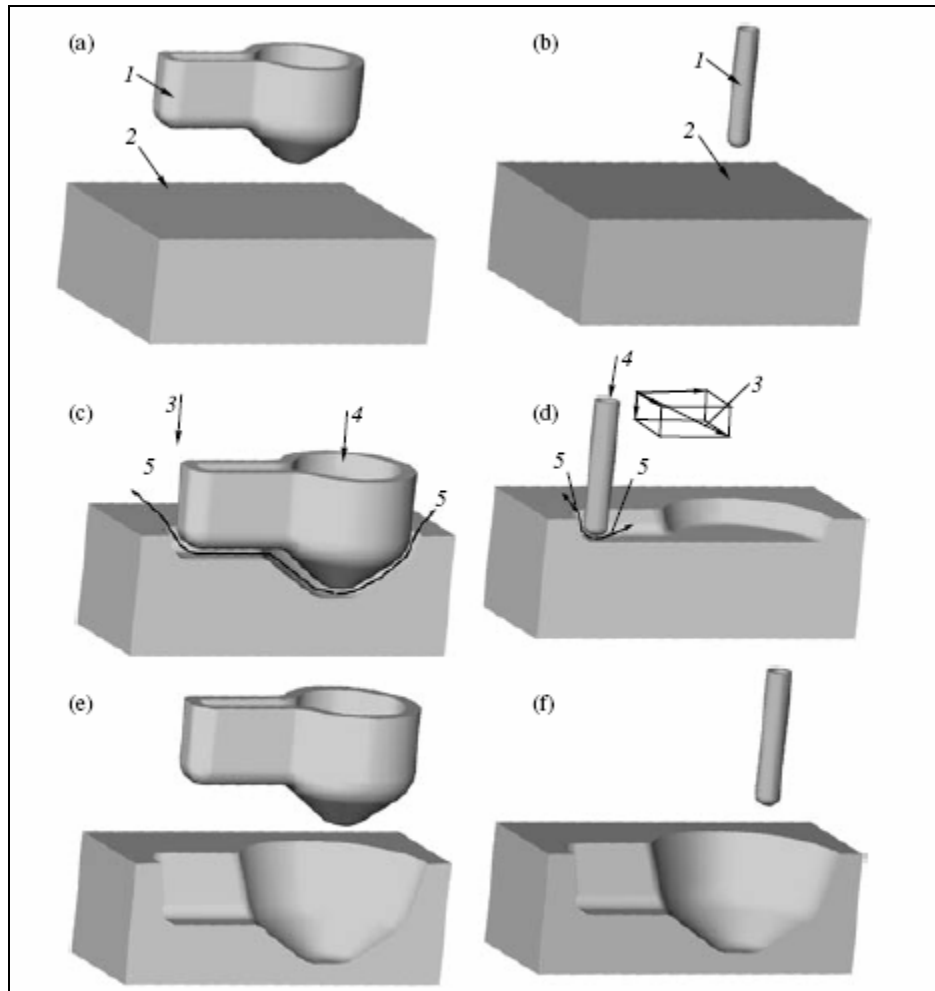


*Figure 3*

**Electrochemical shaping (with (a, c, e) shaped and (b, d, f) unshaped tools: (a, b) before, (c, d), during, and (e, f) after shaping. (1) tool, (2) workpiece, (3) tool velocity, and (4,5) entrance and exit of electrolyte) (Davydov, Volgin and Lyubimov 2004)**

## **2.2.1. System Parameters**

The system parameters for microECM can be divided into two sections: static parameters, where the parameters are set one time only and, dynamic parameters, where they change according to system responses.

### **2.2.1.1. Static Parameters**

Static parameters are electrolyte, pulse frequency, tool electrode and workpiece material.

#### **2.2.1.1.1. Electrolyte**

The electrolyte provides optimum conditions for reactions to occur. Once the electrolyte is set, it can be used several cycles, provided that it has being filtered out of reaction products continuously and the concentration remains constant. An ideal electrolyte has high conductivity, low viscosity, non-corrosive and cheap. There are many types of electrolytes as well there are many concentration and flow rate combinations. Concentration and flow rate studies are done and specific electrolytes for particular purposes have been characterized (Dabrowski and Paczkowski 2005; Davydov, Volgin and Lyubimov 2004; Jain and Rajurkar 1991). Two major types of electrolytes are passive and non-passive electrolytes. Passive electrolytes have oxidizing anions as sodium nitrate. They are environmentally safer and in most times can be used without a fume hood. They provide better precision due to formation of oxide films and oxygen evolution in stray current region. Sodium nitrate is widely used in microECM

processes (Bejar and Eterovich 1995). Non-passive electrolytes contain more aggressive anions as sodium chloride which can require special equipment for use. They remove material faster but the precision is relatively lower compared to passive electrolytes (Bhattacharyya, Malapati and Munda 2005).

The electrolyte can be flushed into the system in three distinct ways. It can be flushed inside and along the tool electrode through a capillary, outside and along the tool electrode or outside sprayed onto the electrodes. Flushing inside the tool electrode has advantage of removing dissolved material right outside where the two electrode cross sections coincide, however it can cause stagnation outside the coincidence. Flushing outside and along the tool, might be disadvantageous electrolyte can turn into turbulent flow at high rates. But it can provide much more fluid flow at lower pressures. Finally, flushing onto the tip of the tool electrode, is easier to set up, but may not yield a cleaning zone as constrained as others. *Figure 4* presents scanning electron microscopy (SEM) images of the holes machined on a stainless steel plate using different electrolytes.

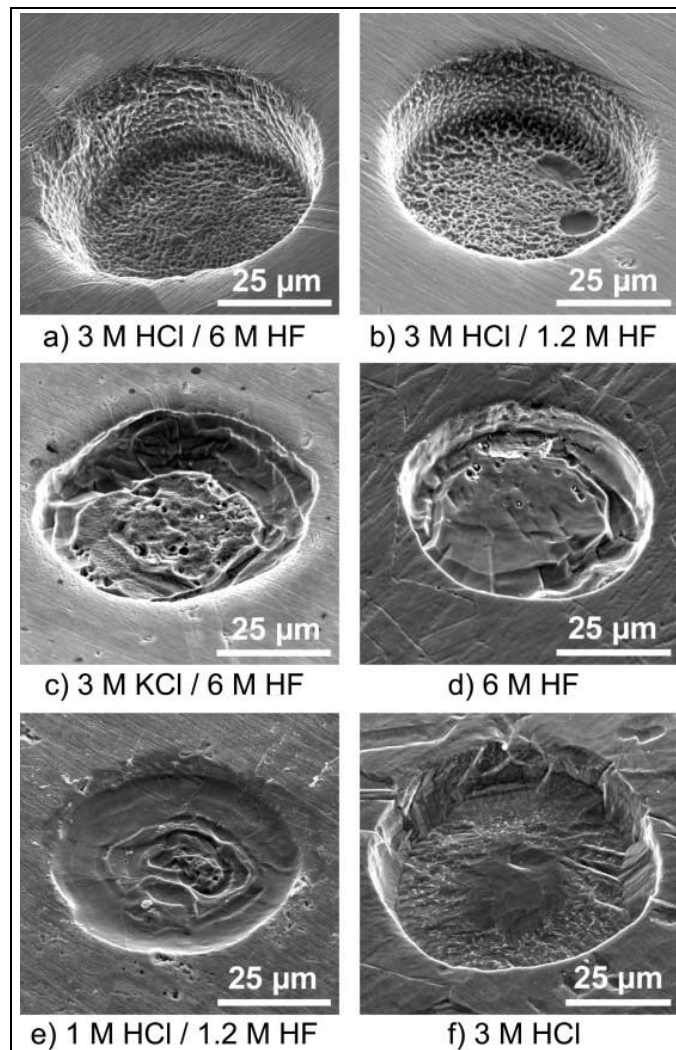


*Figure 4*  
**Comparison of holes drilled into stainless steel in different electrolytes (Cagnon et al. 2003)**

#### **2.2.1.1.2. Pulse Frequency**

Electrochemical machining conventionally utilizes DC input as power source. Novel techniques however employ high frequency pulsed voltage to reach better resolutions. The applied voltage waveform plays a crucial role in defining a profile quality and surface finish of microECM'ed part. In the last decade, ultrashort pulse

microECM has been studied (Schuster et al. 2000; Amalnik and McGeough 1996; Bhattacharyya and Munda 2003; Kozak, Rajurkar and Wei 1994; Maeda, Chikamori and Yamamoto 1984). With the use of ultrahigh frequency inputs around GHz range, electrochemical reactions are restricted to electrode regions in close proximity which exceeds far beyond the 0.1mm limited spatial resolution defined solely by electrolytic current density in DC voltages (Schuster et al. 2000). This application resulted in increasing accuracy but reducing machining efficiency. Machining is performed during pulse-on time and pulse-off time is kept long enough to dissipate heated electrolyte and produced gas formed during pulse-on time. The material removal is decreased due to highly confined electron motion, eventuating a major problem in ultrashort pulsed systems (Davydov, Volgin and Lyubimov 2004; Kenney and Hwang 2005).

The relatively small inverse polarity is required on pulsed systems to promote the possible dissolution of plated product on the tool electrode during an inverse pulse (Zhou et al. 1997; Uhlmann et al. 2001).

A schematic effect of pulse duration is given in *Figure 5*. With higher frequencies, the machined cavity diameter converges to the tool diameter.

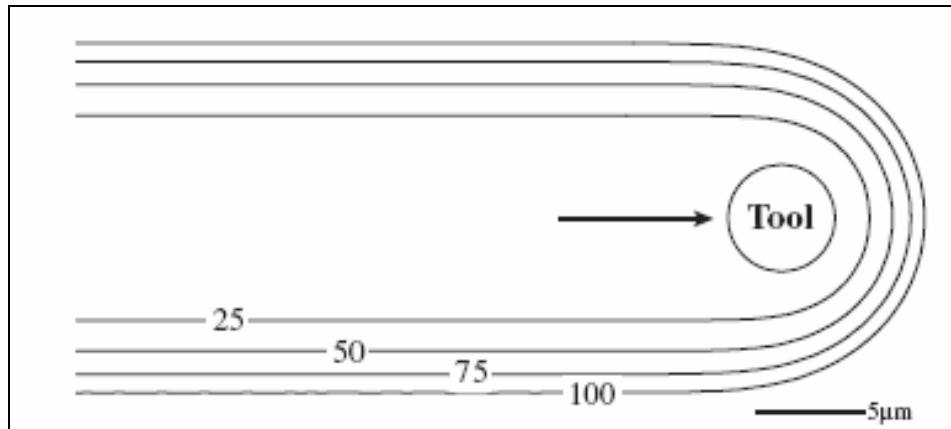


*Figure 5*

**Feature profile evolution of a lateral etch on substrate ( $5 \mu\text{m}$  diameter tool moving at  $1.5 \mu\text{m min}^{-1}$ . Pulse durations as indicated (ns)) (Kenney and Hwang 2005)**

On the other hand, increased amplitude would increase the removed material for a given time, since more electrons are driven with more power supplied. Combined effect of ultrashort voltage pulses and voltage amplitude is well studied (Cagnon et al. 2003). *Figure 6* shows the matrix relations of pulse duration of 50-200ns (20-5MHz) and amplitude of 1.5-4 V.



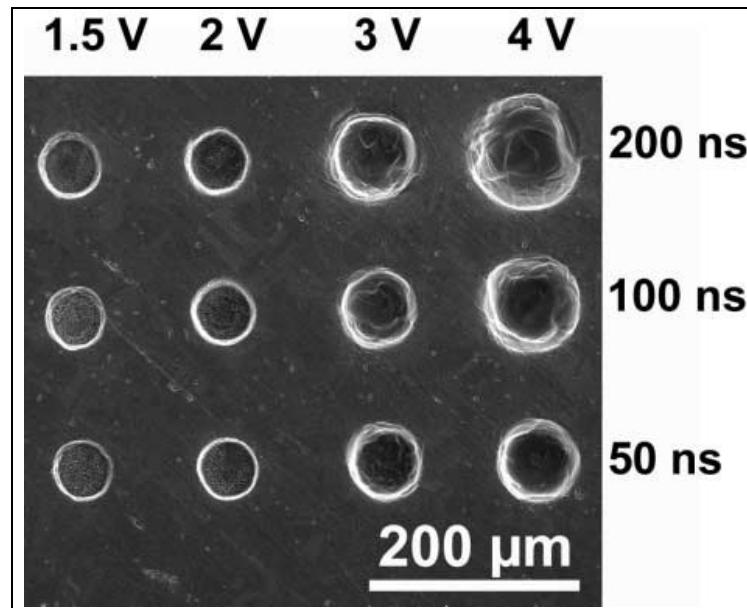


*Figure 6*

**Array of holes drilled with different pulse parameters into stainless steel (Cagnon et al. 2003)**

#### **2.2.1.1.3. Tool Electrode**

As addressed before, shape of tool electrode defines shape of workpiece product. Therefore, the tool electrode shaped or unshaped, once machined, can be used for a long time, since no tool wear is expected in this process. The tool electrodes are machined depending on the application. Smaller electrodes can be shaped by other micromachining techniques.

Most of the machining takes place on the front end of the electrode since there is a stronger electrical field. However, as the tool machines into the workpiece, sidewalls of the tool also start facing the inner walls of the workpiece. This introduces an extra portion of the current distribution, which results in higher machining rates in the entrance sides. To avoid this problem, tool sidewall insulation is developed. The effect

of tool electrode diameter and insulation is studied by Park, Kim and Chu (2006).

Tapered sidewall formation is depicted in *Figure 7*.

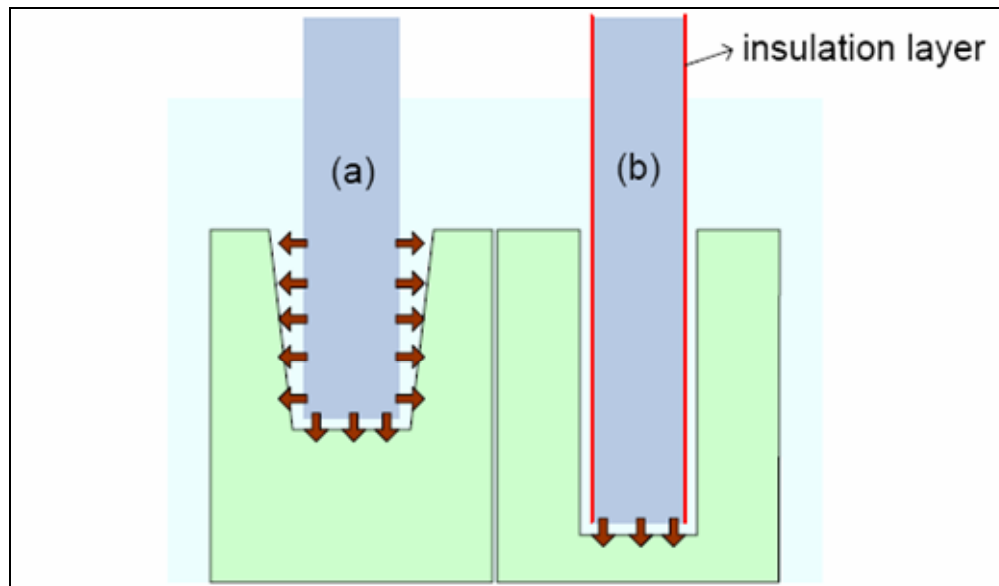


*Figure 7*

**Side effect (with (a) uninsulated, (b) insulated tool) (Park, Kim and Chu 2006)**

Side effect problem is also investigated by Sen and Shan (2003) as conicity. The problem is apparent in the cross sectional SEM view of a hole drilled, shown in *Figure 8*.

Also, bigger tool electrode implies an augmented rising time of the potential within the pulse. Therefore, the potential does not rise fast enough within the short pulse duration when the diameter is larger. This decreases the machining rate. A study result is shown in *Figure 9*.

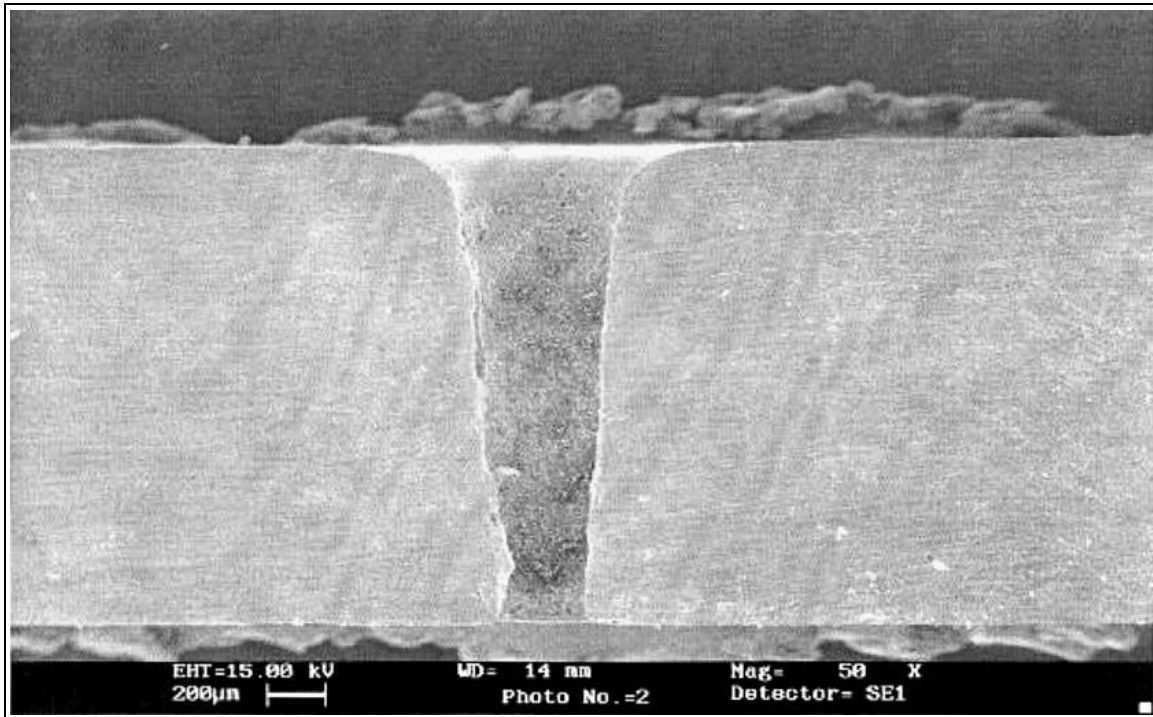


*Figure 8*  
 Longitudinal cross-section of drilled hole (0.1 M H<sub>2</sub>SO<sub>4</sub> electrolyte, SUPERNI 263A alloy workpiece) (Sen and Shan 2003)

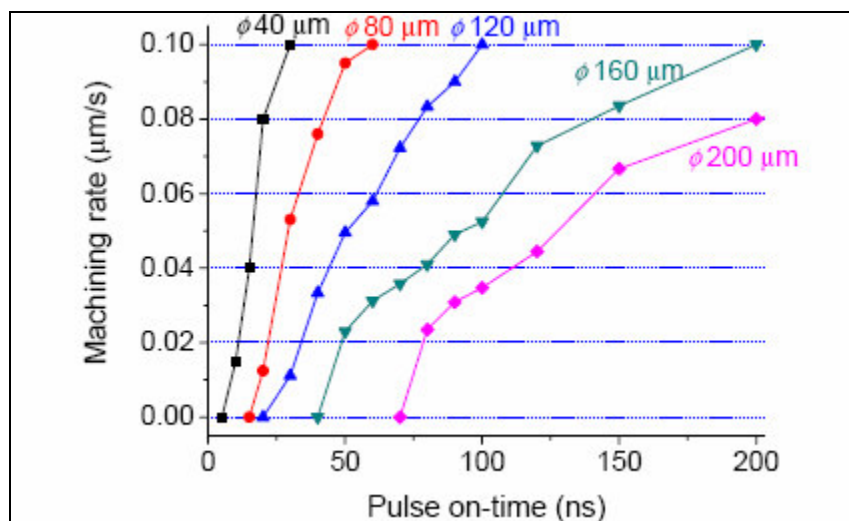


*Figure 9*  
 Effect of tool electrode diameter on machining rate (0.1 M H<sub>2</sub>SO<sub>4</sub> electrolyte, stainless steel 304 workpiece) (Park, Kim and Chu 2006)

Multiple micro features can be drilled using two approaches. First, a single tool electrode can be programmed to repeat a certain motion to produce multiple holes. Or multiple tool electrodes could be used to machine at once, which would be a faster method.

Single microprobes for tool electrode applications were machined by dissolving tungsten carbide utilizing same electrochemical processes (Lee, Baek and Cho 2007). The electrodes produces are illustrated in *Figure 10*.

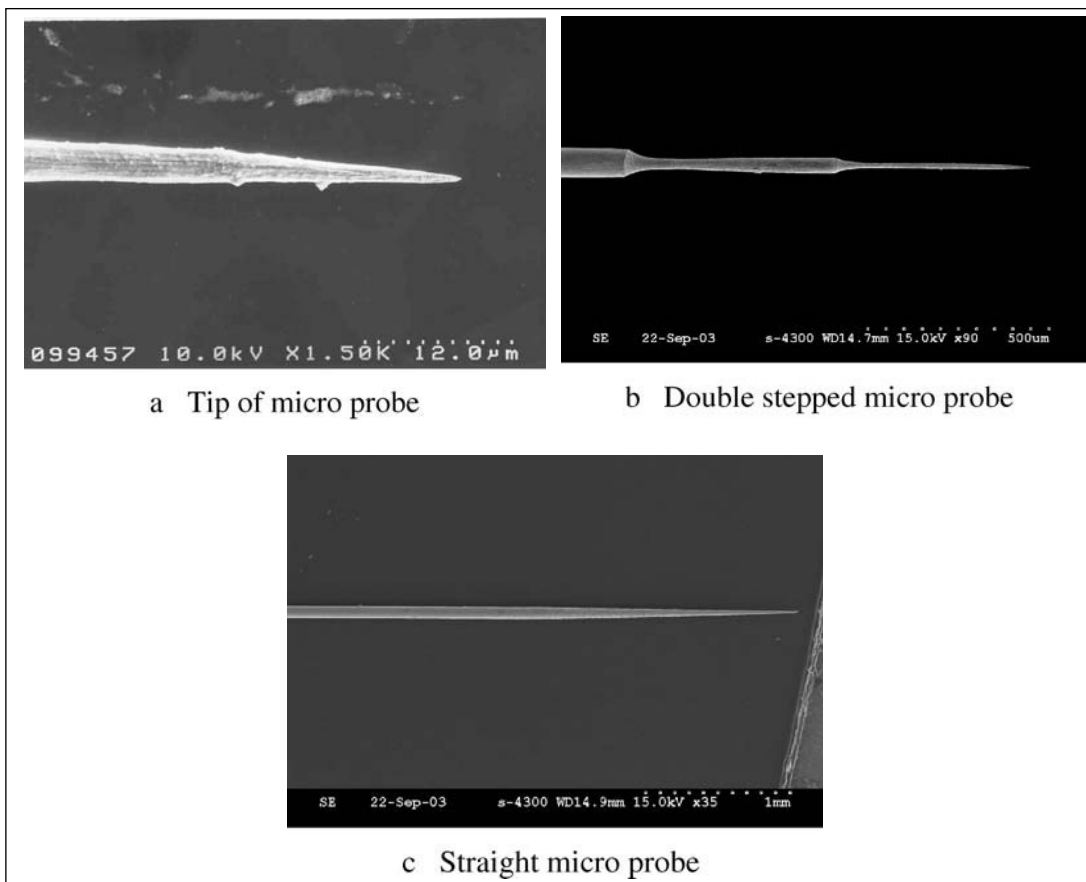


*Figure 10*  
**Examples of microprobes (Lee, Baek and Cho 2007)**

For improved flushing conditions and shape accuracy, vibrating tool electrode has been used by researchers (Förster, Schoth and Menz 2005). Tool electrode is fed towards the workpiece in a superimposed oscillatory motion.

#### **2.2.1.1.4. Workpiece Material**

Workpiece material is also a static parameter. The choice of material is primarily dependent on the application. Mechanical and biological factors are considered for specific purposes. For workpiece material, the only condition is to be conductive. Molecular weight of dissolved workpiece material and dissolution valence have explicit effect in material removal rate (Datta 1998). Higher the dissolution valence, lower the material removal rate.

Material selection is also important depending on the use of electrolyte. Some electrolytes such as sodium chloride cannot be used on tungsten carbide or molybdenum since they are corrosive and produce large amount of sludge.

Some other passive electrolytes such as sodium nitride are good on aluminum, stainless steel or copper. Material removal is however independent of material hardness (Benedict 1987).

#### **2.2.1.2. Dynamic Parameters**

Dynamic parameters are inter electrode gap, resistance and current density.

#### **2.2.1.2.1. Inter Electrode Gap**

Inter electrode gap (IEG), also known as machining gap, is defined as the frontal gap between the tool electrode and workpiece surface. The two electrodes are circuited through the electrolyte flowing from tool electrode to workpiece electrode. To invoke localized anodic dissolution, the tool electrode is brought to the proximity of workpiece electrode and the IEG has been reduced as much as possible within the limits of actuators and measurability (Rajurkar et al. 1999). Specific IEG is around 10-25  $\mu\text{m}$  and is being reduced to sub-micron level with the use of piezo-driven stages and sub-50  $\mu\text{m}$  diameter cylindrical wires (Schuster et al. 2000). Material removal rate (MRR) is relatively increased this way by providing a vertical removal giving a deeper slot or a hole. This is due to the confined machining zone, where electron mobility is restricted to the IEG.

The dynamic of IEG depends on the actuation mechanism. It can be reduced further by driving the tool electrode towards the workpiece, or can be increased by pulling it back.

#### **2.2.1.2.2. Resistance**

Resistance to applied current is based on the electrolyte resistivity. This is the resistance shown on a unit distance. Since the distance is involved, it provides a function of IEG and current density and explained in detail in the theory section. The columnar electrolyte flow from the tool electrode to workpiece can be analogized to a wire with a known diameter that carries a current. It exhibits a resistance across the cross section of

the wire and against the length of the wire. Hence it is inversely proportional to the length of the wire.

Electrolyte resistivity also changes depending on the electrolyte type and concentration. By reducing salt concentration in passive electrolytes, resistivity is increased and the inter electrode gap can be reduced to achieve better precision. In acidic electrolytes concentration is reduced by addition of additive chemicals like  $\text{NaHSO}_4$ , which has the same effect on resistivity (Bhattacharyya, Malapati and Munda 2005).

#### **2.2.1.2.3. Current Density**

Current density is the electrical current distributed over the electrode projected area. An ammeter is serially connected to the system. As will be defined later on, current density is related to the IEG. At smaller electrode gaps, the power supplied is distributed on a smaller area, providing a denser effect. Since, the IEG is stated as a dynamic parameter, so is the current density. The current density also relates to the voltage supplied and increases with higher voltage driven to the system. Parametric studies investigating effect of machining gap on current density were carried (Mukherjee, Kumar and Srivastava 2005). *Figure 11* shows such a relation.

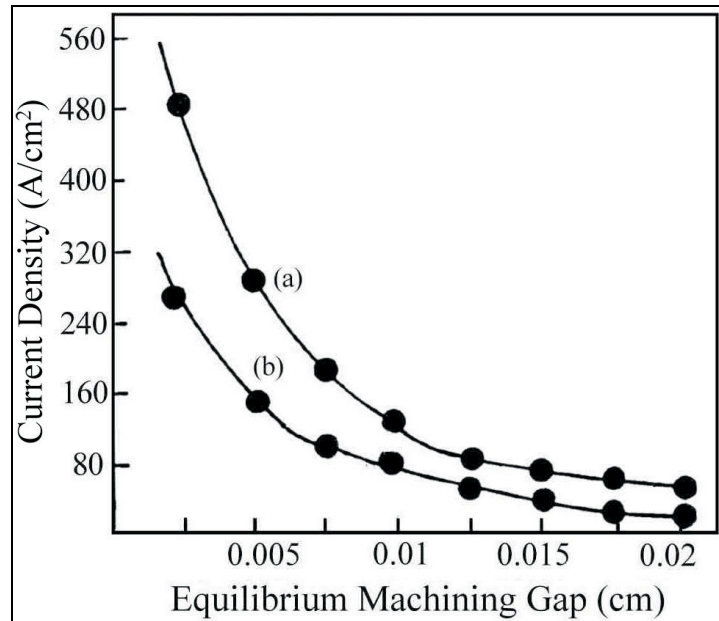


Figure 11

Variation of current density with equilibrium machining gap ((a) for actual current density (b) for over-potential corrected current density) (Mukherjee, Kumar and Srivastava 2005)

## 2.2.2. Theory

### 2.2.2.1. Current Density and IEG Relation

Theoretical background for the current density and inter electrode gap relation, is based on the Butler-Volmer equation (Bard and Faulkner 1980). The equation explains that in electrochemical processes, the over-potential  $\varphi$  is in an exponential relation with current density. Over-potential is defined as difference in the electric potential of an electrode with no current flowing through it, and with a current flowing.

$$i = i_0 \exp\left(\frac{\beta n F}{R_g T_a} \varphi\right) \quad (3)$$



where,

$i$ : dissolution current density ( $A/m^2$ ),

$i_0$ : exchange current density at equilibrium ( $A/m^2$ ),

$\beta$ : charge transfer coefficient,

$n$ : number of valence electrons,

$F$ : Faraday constant,

$R_g$ : gas constant,

$T_a$ : electrolyte temperature ( $^{\circ}K$ ),

$\varphi$ : over-potential (V).

Applying, Ohm's law,

$$i = \frac{E(t)}{gr} \quad (4)$$

where,

$E(t)$ : applied voltage (V),

$g$ : the tool electrode workpiece gap or IEG (m),

$r$ : electrolyte resistivity ( $\Omega\text{-m}$ ).

Equations (3) and (4) show the inversely proportional relationship between the IEG and the current density.

### 2.2.2.2. Material Removal Rate

Formulation for MRR uses Faraday's first law, stating the proportionality of the removed mass to the current across the electrodes (Datta 1998).

$$R = \frac{IM}{nFA\rho} \quad (5)$$

where,

$R$ : material removal rate (cm/s),

$I$ : current (A),

$M$ : molecular weight of the dissolved material (g/mole),

$A$ : tool frontal end surface area (cm<sup>2</sup>),

$\rho$ : material density (g/ cm<sup>3</sup>).

Applying equation (4) on (5) and normalizing to current by multiplying with area, theoretical MRR over a pulse-on duration is defined as,

$$V = \int_0^{\tau} \frac{MEA}{nF\rho gr} dt \quad (6)$$

with,

$$C = \frac{M}{nF\rho} \quad (7)$$

$C$ : specific removal rate (mm<sup>3</sup>/A-s),

$\tau$ : on-pulse duration.

Substituting (7) in (6), single pulse-on material removal rate is obtained as:

$$V = \int_0^{\tau} \frac{CEA}{gr} dt \quad (8)$$

The feed rate  $f_r$ , the rate at which the electrode can be driven towards the workpiece, is defined by the following combined equation,

$$f_r = \frac{V}{At} = \frac{CE}{gr} \quad (9)$$

### 2.2.3. MicroECM Applications

MicroECM can be applied to hole drilling, grinding, feature shaping, and deburring.

#### 2.2.3.1. Hole Drilling

MicroECM is an effective method for drilling holes. Single holes or a series of holes can be drilled either by using a single tool electrode and actuating it several times to repeat the job, or a custom multiple tool electrode to save time dramatically (Park and Chu 2007). The holes were drilled in an open-loop actuation controlled setup. Pulse-on time and the period were 110ns and 3.2 $\mu$ s respectively. Multiple through hole images are shown in *Figure 12* and a zoomed hole in *Figure 13*.

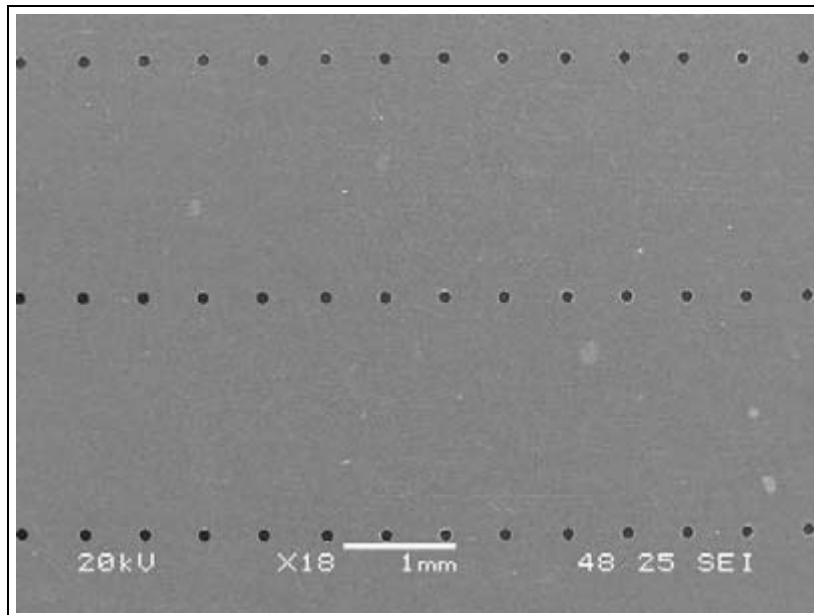


*Figure 12*  
**Micro hole array (0.1 M H<sub>2</sub>SO<sub>4</sub> electrolyte, 304 stainless steel workpiece) (Park and Chu 2007)**

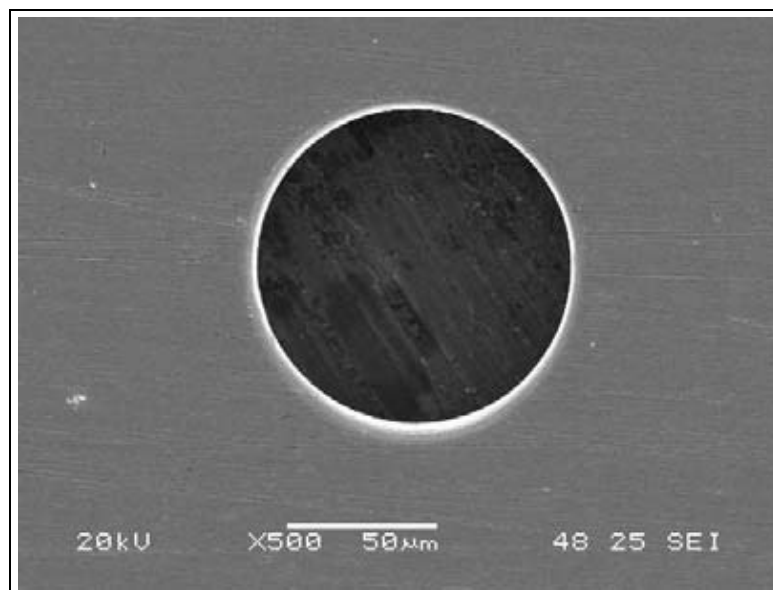


*Figure 13*  
**Hole close view (0.1 M H<sub>2</sub>SO<sub>4</sub> electrolyte, 304 stainless steel workpiece) (Park and Chu 2007)**

MicroECM hole drilling approach is widely used in producing ink-jet nozzles. Electroformed nozzles are nickel plated on a mandrel mold, forming nozzle pattern (Datta 1995). Entry/exit hole formation is the principle behind the ink-jet printing technology, where entry holes are defined to be the holes machined with initial tool action approaching to the workpiece. Exit holes were formed when the tool exit and leaves the plate after machining a through hole. A 55  $\mu\text{m}$  diameter photoresist opening was patterned on a 25  $\mu\text{m}$  thick foil. The 55  $\mu\text{m}$  diameter exit hole diameter was achieved with a low standard deviation of 2.0. Nozzle angle of  $27^\circ$  was machined through etching. *Figure 14* illustrates those two types of holes machined using microECM technology.

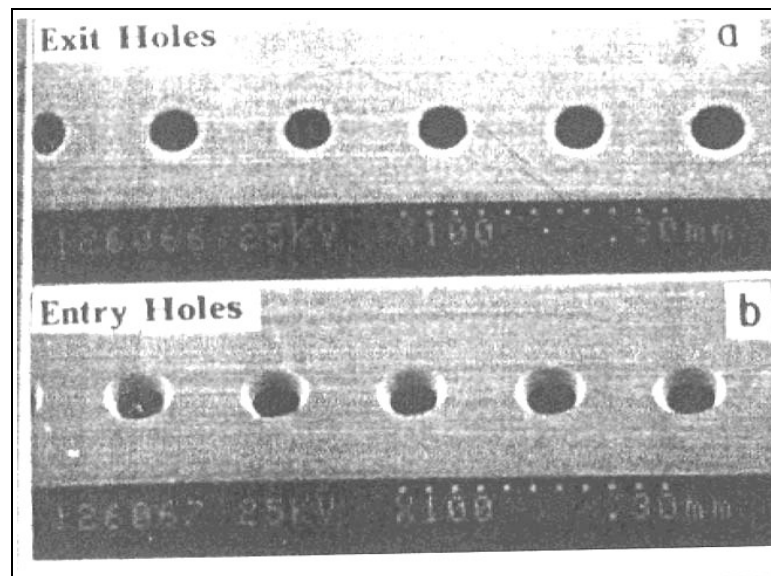


*Figure 14*

**Canonical nozzle ((a) entry holes, (b) exit holes, NaCl and glycerol mix electrolyte, stainless steel workpiece) (Datta 1995)**

### 2.2.3.2. Grinding

Electrochemical grinding (ECG) appeared as a variation of ECM systems. The material removal is achieved using both mechanical and electrochemical abrasive actions. A rotating wheel is the cathode in ECG. Rotation of the grinding wheel helps dispersing the electrolyte fluid around the machining zone. At very high speeds, the MRR goes up to certain point, after which the electrolyte pressure is not enough to keep the fluid around the machining zone due to large centrifugal force applied (Tehrani and Atkinson 2000). An illustration of the ECG system is given in *Figure 15*.

Electrochemical grinding is a very fast technique for producing burr-free cut-off. Low induced stress and heat-free machining are the advantages shared by the microECM systems.

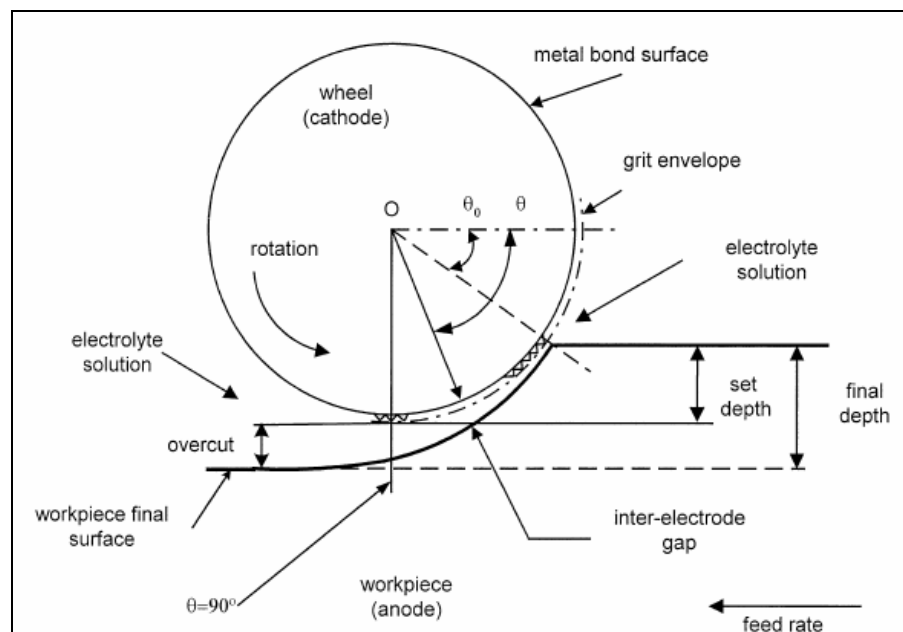


*Figure 15*  
**Electrochemical grinding process (Tehrani and Atkinson 2000)**

### 2.2.3.3. Feature Shaping

MicroECM technology can be used to machine more complex shapes. Material removal can be achieved using either a multi axial actuation mechanism and an unshaped tool electrode or a custom shaped tool electrode and less degree of freedom actuation. This way multifarious 3D features with high aspect ratios can be shaped. Multi axial actuation using an unshaped tool electrode was performed using a cylindrical Pt wire of 10  $\mu\text{m}$  diameter (Schuster et al. 2000). The tool first advanced onto the Cu workpiece and then moved along a rectangular path analogous to a micro milling cutter tool. Scanning electron micrographs of the structures are shown in *Figure 16*.

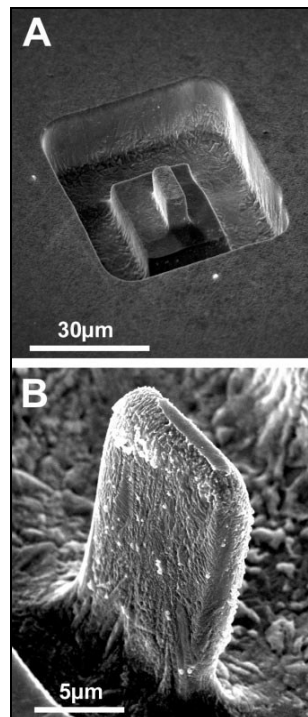


*Figure 16*

(a) 3D Cu structure and (b) Cu tongue, (2 MHz, 1.6 V, 10  $\mu\text{m}$  Pt wire tool, 0.01 M  $\text{HClO}_4$  and 0.1 M  $\text{CuSO}_4$  electrolyte) (Schuster et al. 2000)

A faster approach, single degree of freedom machining, is possible by customizing a tool electrode, so it will project the inverse geometry on the workpiece. Such studies are common (Förster, Schoth and Menz 2005; Kirchner et al. 2001). *Figure 17* shows a tool electrode and microECM machined cavity.

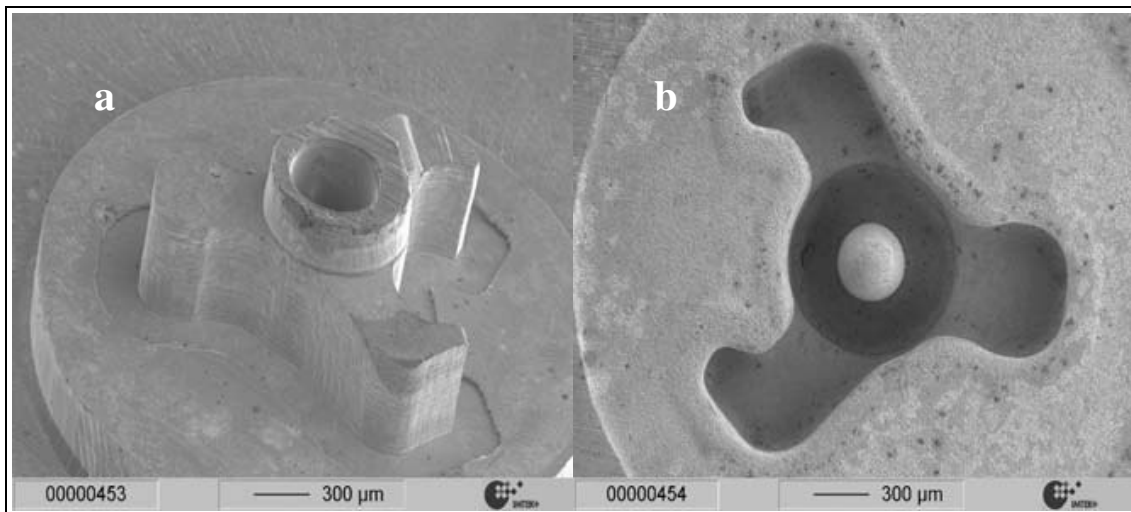


*Figure 17*

**(a) Tool electrode and (b) machined cavity (50 Hz, 0.2 mm amplitude,  $\text{NaNO}_3$  electrolyte, brass tool, hot forming tool steel workpiece) (Förster, Schoth and Menz 2005)**

*Figure 18* depicts a freestanding microcantilever which is a very common device in Microsystems. Both features were machined using a custom shaped electrode and uniaxial actuation mechanism.



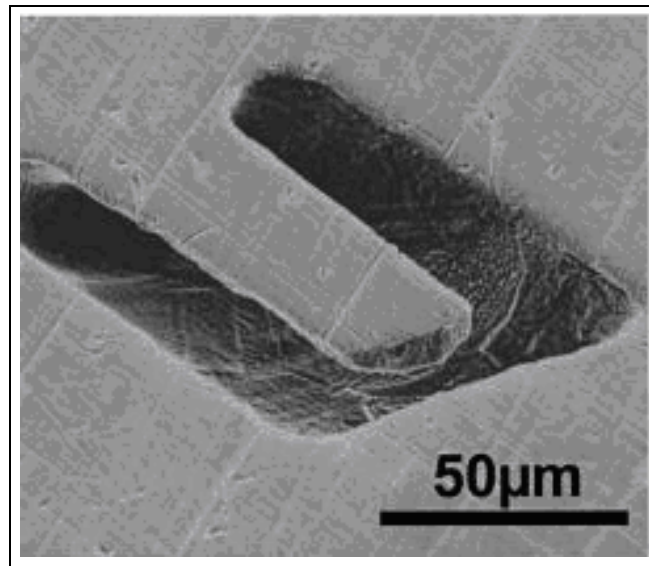


*Figure 18*  
**Freestanding microcantilever machined into stainless steel sheet (Kirchner et al. 2001)**

#### **2.2.3.4. Deburring**

MicroECM is a suitable technology for removing burrs made by other operations. The burrs on the machined edges are removed using a flat tool electrode that faces the burrs and brought into close proximity as in regular microECM processes. Since the tool shape is projected, a flat shape yields a smooth, burr free surface finish. It is a very fast method for deburring. It is observed during a removal of a 25  $\mu\text{m}$  high burr above a  $\text{Ø } 400$  punched hole. Deburring took place in about 0.5 s with a flat tool electrode positioned 100  $\mu\text{m}$  above the workpiece (Osenbrugger and Regt 1985). *Figure 19* shows an industrial deburring application.

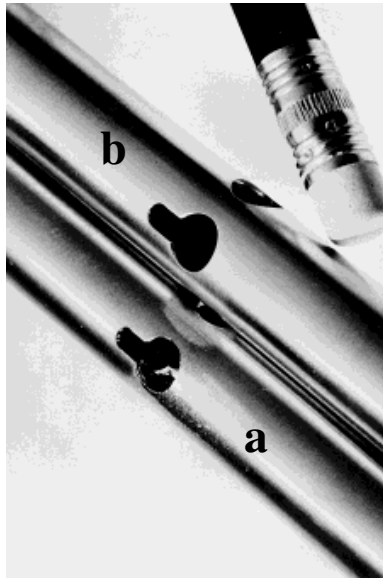


*Figure 19*

**(a) Machined piece with burrs and (b) deburred piece (Vectron Deburring 2006)**

#### **2.2.4. System Control**

MicroECM setups mostly have actuation mechanisms for repeatable machining. Two types of actuation is possible on a setup and they define types of control mechanisms as well: open-loop and closed-loop controls.

##### **2.2.4.1. Open-loop Control**

Open-loop actuation is applied when an actuation command is executed once without taking any system response into consideration. Specifically for microECM, the tool electrode can be advanced onto the workpiece at a constant feed rate which can be experimentally determined for a set of parameters such as material, electrolyte, input power, etc. Although direct and simple, it is less accurate since it does not consider any

system behavior or disturbance. If material removal is not fast enough as anticipated (e.g., contaminated electrolyte, non-uniform microstructure in workpiece, or non-uniform electrolyte flow), the the tool can touch the workpiece and cause short circuiting. This would create burns and micropits on the surface which would badly affect the surface quality and feature profiles (Bhattacharyya, Malapati and Munda 2005).

Open-loop system can be advantageous when all the parameters are predefined and system is expected to exhibit no or very little disturbance. The system does not take any measures for simply two reasons: lack of sensing mechanism for possible changes, and lack of algorithms to computerize the response and make decisions.

#### **2.2.4.2. Closed-loop Control**

Closed-loop control is an approach to avoid detrimental effects which open-loop actuation can cause due to narrow IEG in microECM. Closed-loop control requires a feedback mechanism where meaningful data could be gathered for process monitoring. Then corrective measurements could be taken depending on the feedback information. Process monitoring is maintained gathering feedback signals for microECM.

One feedback mechanism for the microECM is using the current flow through the electrolyte in IEG. As introduced in equation (4), the current density on the frontal electrode area is inversely proportional to the tool separation itself. Therefore a current reading, with a known tool diameter could provide coherent data for tool position. A sudden jump in current density would mean the tool is approaching workpiece fast and a

possible corrective measure could be taken such as, holding the tool in stand-by mode until the current density drops under a certain value.

Electrical current is quite popular and used for monitoring microECM processes. (De Silva and McGeough 1998; Yong et al. 2003; Chikamori 1998). For such systems, an ammeter is serially connected to the system to record current through the electrolyte flowing in between tool electrode and workpiece. Such a system is designed and developed by Zhang et al. (2007) and can be seen in *Figure 20*.

Actuation mechanism of such system can range from piezo drivers to DC motors depending of the resolution requirements.

Typically, once the feedback signal is acquired, it is sent to the control unit, which can be simply a PC or an industrial control unit. The data is evaluated, and actuation signals are generated. The signals are sent to the actuator controller unit which then drives the actuators.

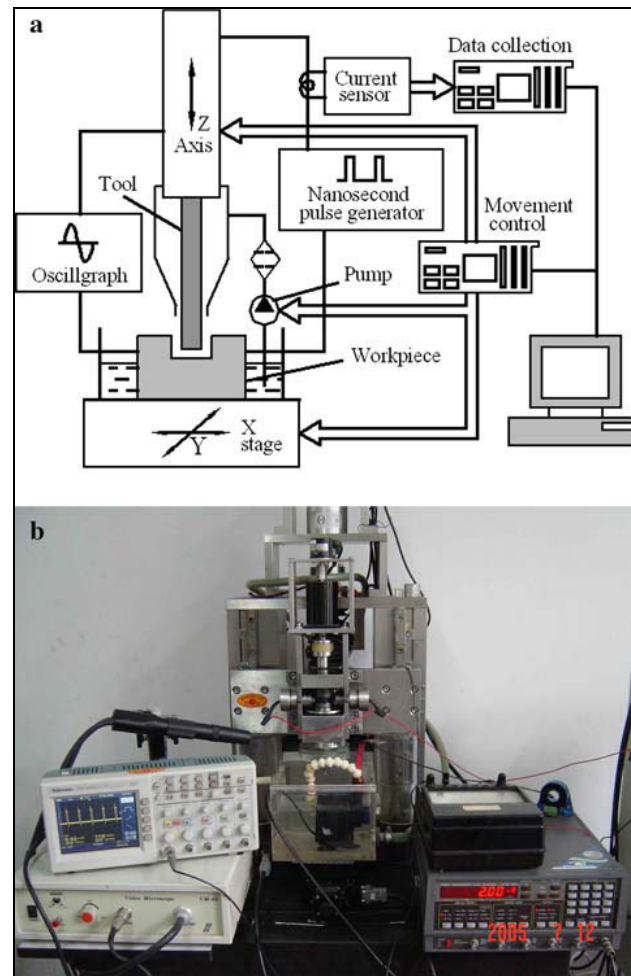


*Figure 20*  
**Developed pulse micro-ECM system ((a) schematic diagram and (b) photo) (Zhang et al. 2007)**

Closed-loop control, generally deals with system dynamics as position, velocity and acceleration. Most of the systems which deal with piezo drivers or stepping actuation, do not have a velocity or acceleration control loop in the local sense. Most general control loop is done by controlling the position of the tool electrode. Since the tool electrode position is varying, the current should be brought to a set point and used as a constant determination. Constant current position control is adequate for many

systems and corrective actuation measurements are taken depending on the unexpected current jumps.

Some control algorithm is based on binary logic, where the decisions are made after yes/no decisions and if/else questions. The algorithm is looped until a certain pre-determined value is reached. *Figure 21* illustrates such a flowchart. Different control algorithms such as fuzzy logic are also possible depending on the application and actuation mechanism (Skrabalak, Skrabalak and Ruszaj 2004).

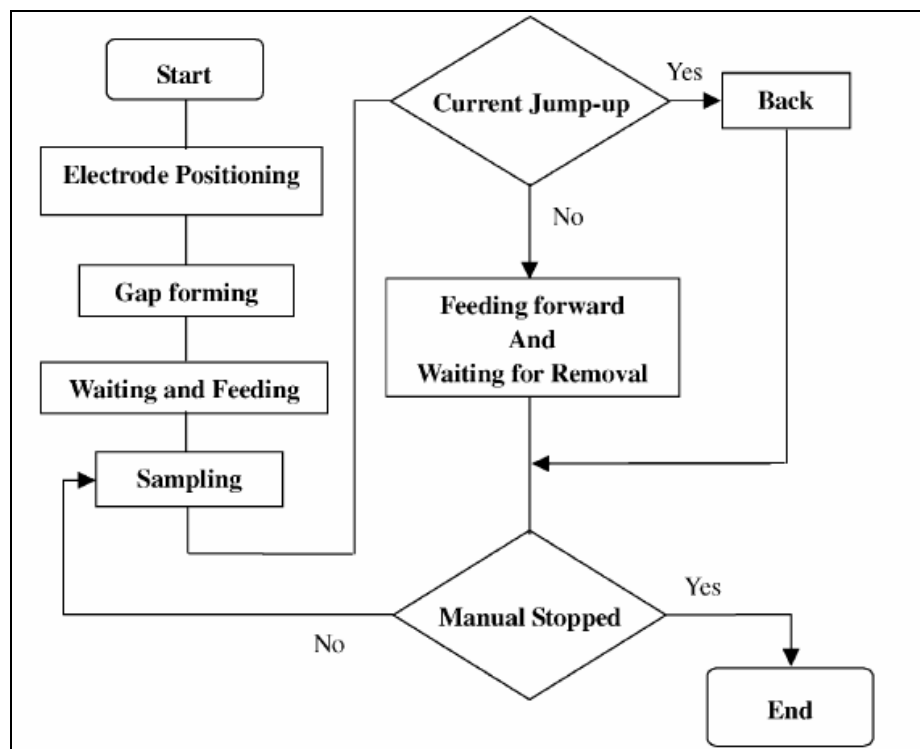


*Figure 21*  
Flow chart of gap control (Yong et al. 2003)

### 2.2.4.3. PID Control

Many industrial controllers are hydraulic, electronic or pneumatic controllers. Different types of control actions are required for different actuation and sensing mechanisms. However, most of the industrial control systems follow similar block diagram, having a plant, actuator, sensor and automatic controller (Ogata 1997). *Figure 22* shows a block diagram of a control system. Initially a set point is given to the system. The signal is amplified and modulated to the desired level, then actuation mechanism works and changes are reflected to plant, which yields the output. Output signal then is sensed via a sensor mechanism and compared to the reference input. If any difference occurs, signal is controlled via amplifier again and another output is yielded. The loop continuous to meet the criteria defined by set point.

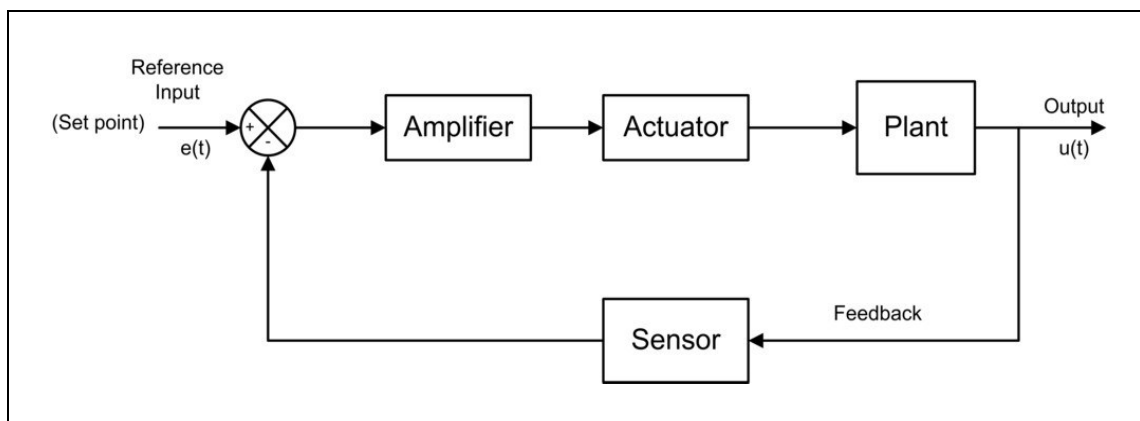


*Figure 22*  
**Generic control system**

Proportional-Integral-Derivative (PID) control is widely used in industrial applications (Brogan 1985; Dorf 1992).

Proportional P control has the following relation between output controller  $u(t)$  and input error signal  $e(t)$ .

$$u(t) = K_p e(t) \quad (10)$$

where,

$K_p$ : proportional gain constant

Proportional control is basically an adjustable gain amplifier. The relationship between output  $u(t)$  and actuator error signal  $e(t)$ , in an integral controller is given as:

$$u(t) = K_i \int_0^t e(t) dt \quad (11)$$

where,

$K_i$ : integral gain constant

Integral control action is taken to eliminate the actuation error. The relationship between output  $u(t)$  and actuator error signal  $e(t)$ , in a derivative controller is given as:

$$u(t) = K_d \frac{de(t)}{dt} \quad (12)$$

where,

$K_d$ : derivative gain constant

The derivative action introduces damping to the system and eliminates any overshoot behaviour.



Proportional, Integral and Derivative control actions can be individually taken or combined in different ways. Output-input Laplacian relationship of a PID controller can be stated as follows:

$$\frac{U(s)}{E(s)} = K_p \left( 1 + \frac{1}{T_i s} + T_d s \right) \quad (13)$$

where,

$T_i$ : integral time

$T_d$ : derivative time.

### 3. SYSTEM PROCESS CONTROL

Designing the process control was based on the consideration of following:

- High repeatability
- High accuracy
- Low hysteresis
- Low cost
- Least computation time
- Flexible for new instrument inclusion

PID control, defined in previous section, has the following advantages over a sample step input:

- Almost zero error signal
- Overshoot damping
- Short rise time
- Reduced oscillations

However, it generally applies to continuous actuation systems such as DC electric motors, AC electric motors, hydraulic systems, pneumatic systems, etc. In the case of stepping actuation, PID control with derivative and integral action would not benefit the system. Since the step actuation is uninterrupted in a step time, the control methodology remains in a more general frame. For instance, overshoot can happen not in a single step but as a few steps on a 1000 steps actuation range. The overshoot and

oscillation behavior is device dependent in stepping actuation mechanisms and can be taken care of by designing smaller step size, low backlash gear modules.

Binary logic control, on the other hand, is an industrial control platform which performs, fast and reliable control for automatic systems. Industrial control is based on on/off actuations and highly suitable for stepping actuation which is an on/off binary actuation. Less computation time, high reliability and robust actuation is provided using binary logic control.

A high frequency closed-loop microECM system was designed. A waveform voltage bias is supplied across the electrodes by a high frequency function generator. An amplifier is used to modulate the voltage amplitude beyond the limits of the function generator. Tool electrode is negative terminal and workpiece electrode is positive terminal. An ammeter is serially connected to the system. The signals acquired from the ammeter for current feedback were evaluated on a controlling computer. The input output (I/O) communication is provided over serial communication ports through a serial instrument controller interface board. The output signal was manipulated as per input evaluations and sent to actuators to complete the required action. The instrument schematic is illustrated in *Figure 23*.

Inversely proportional relationship principle between the IEG and the current density is utilized. Decreasing the electrode gap causes an increase in the output current density; the current change would then provide informative data of the electrode position.

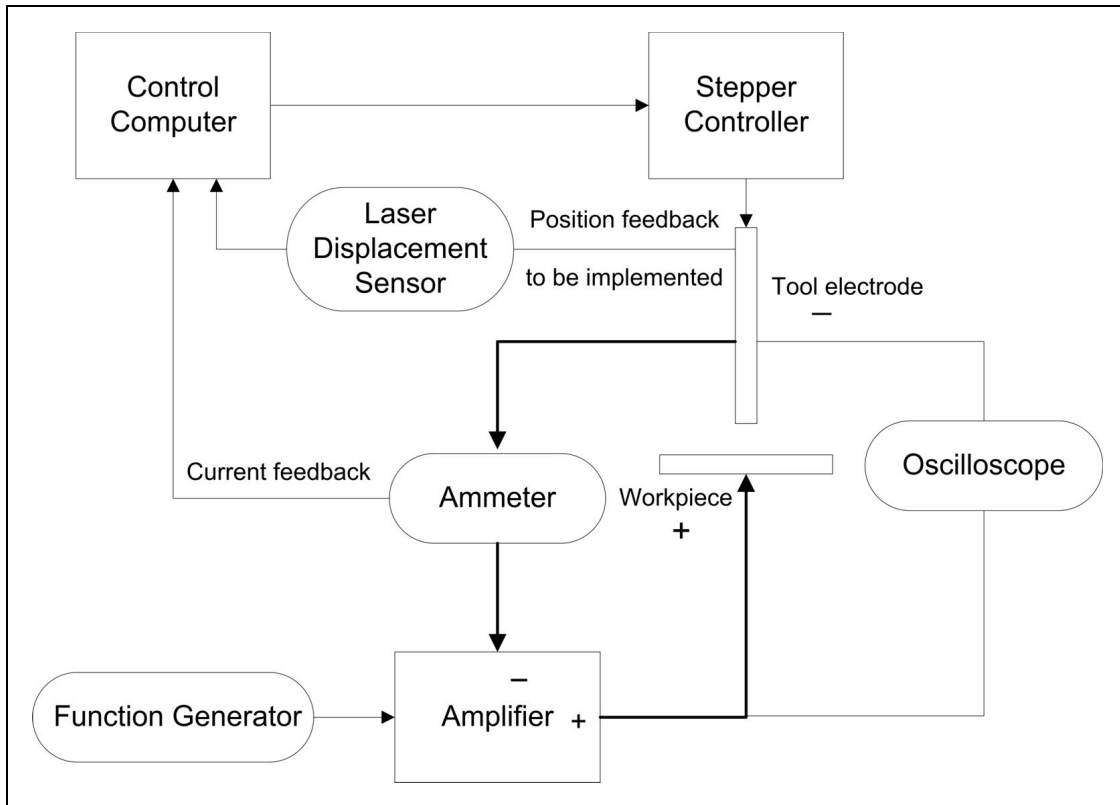


*Figure 23*  
**Current and position feedback design**

Controlling algorithms for closed-loop experiments were constructed using a binary logic approach. If and else conditions were primarily questioned and corresponding measures were taken. The control logic data flow is depicted in *Figure 24*.

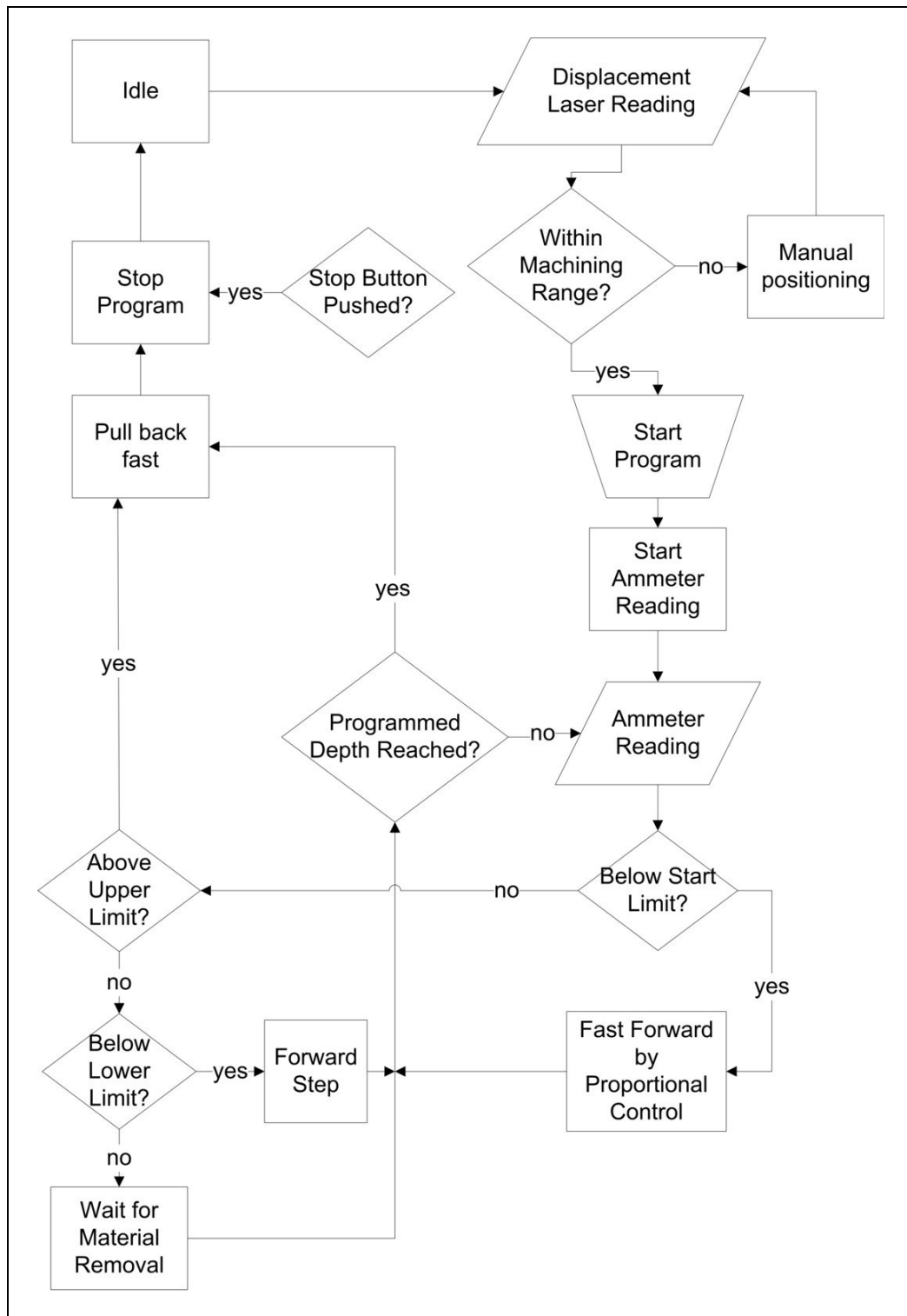


*Figure 24*

**Flow chart of tool electrode position and velocity control**

The sequences of control algorithm are given as follows:

- 1) Initially displacement sensor output data is checked to see if the tool is in active machining proximity or not. If the laser is in the range, the program is started with ammeter reading initialization and current value is recorded. If not, the tool electrode is manually forwarded to the reading range and the program is started.
- 2) Current data is recorded as long as the programmed machining is not reached or the stop push button is not pressed. Current values are used to determine decisions and dictate subsequent actions.
- 3) Limit set conditions are determined by the preliminary experiments for calibration purposes, yielding a stable machining current interval. If the present current reading is below the lower value, it is interpreted that the tool is not in machining zone yet; consequently the stepper motor carrying the tool is driven forward in a user defined pace.
- 4) If the recorded data is between upper and lower current reading intervals, system stands by and machining continues. If it is beyond the upper limit, then a fast backward pulling action is executed to separate the tools.
- 5) When the tool reached the desired final machining depth, the system terminates actuation and pulls the tip back to initial home position.
- 6) Initial velocity control is achieved using a similar approach. Given the possibility of starting the program on a random height beyond the reading range of laser sensor, the electrode has been driven in a fast speed determined by user inputted proportional constant until first reading from the laser is recorded. The P control

is achieved multiplying the constant by the regular feed rate to get the fast feed rate.

## 4. EXPERIMENTS

### 4.1. LIST OF EQUIPMENT

The list of equipment used in this study is as follows:

- VXM programmable stepping motor controller and Bi-slide stepping motors.  
Velmex, Inc., 7550 State Route 5 and 20 Bloomfield, NY 14469.
- Agilent 33250A function generator, Agilent Technologies, Inc., 5301 Stevens  
Creek Blvd Santa Clara CA 95051.
- Fluke 45 ammeter, Fluke Electronics, 6920 Seaway Blvd., Everett, WA, 98203.
- TDS 1002B oscilloscope, Tektronix, Inc., 14200 SW Karl Braun Drive P.O. Box  
500 Beaverton, OR 97077.
- LK-G157 laser displacement sensor and LKG-3001V controller, Keyence  
Corporation of America, 50 Tice Blvd., Woodcliff Lake, NJ 07677.
- PCI-8432/4 serial interface board, National Instruments Corp., 11500 N Mopac  
Expwy, Austin, TX 78759-3504.
- XR-p310 audio amplifier, Pioneer Electronics, Meguro, 153-8654, Tokyo, Japan.
- STM6 optical measuring microscope, Olympus America Inc., 3500 Corporate  
Parkway, Center Valley, PA 18034-0610.
- LE26P precision weight balance, Sartorius AG, Weender Landstrasse 94-108  
D-37075 Goettingen, Germany.



Essential instruments employed in microECM setup are detailed further:

#### **4.1.1. Stepper Motors**

Actuation mechanism is maintained by Velmex Bi-slide, stepping motors and Velmex, VXM programmable stepping motor controller. The resolution of the multiaxial system is 2.5  $\mu\text{m}/\text{step}$ . The travel distance of the system is 250mm per axis. It has a load carrying capacity of 300lb. Stepper actuation makes it easy to control the position and velocity of the drives. VXM function is the Pulse Width Modulation (PWM) for  $\frac{1}{2}$  step unipolar motor. Baud rate is settable from 9600 to 38400 depending on communication procedures. The communication is provided by RS-232 Serial Output.

#### **4.1.2. Function Generator**

33250A Agilent function generator yields variable edge and DC waveforms of types sinusoidal, triangular, square or ramp. The frequency can go up to 80 MHz. 12-bit, 200 MSa/s, 64 Kpoint arbitrary waveforms can be generated. AM, FM, PM, FSK, and PWM Modulation, Linear & logarithmic sweeps and burst are standard available. Amplitude ranges from 10m Vpp to 10 Vpp. The device communication is available via GPIB and RS-232 ports. Therefore, all the parameters can be set constant for each experimental run.

#### **4.1.3. Ammeter**

The Fluke 45 dual display multimeter is employed in the system for obtaining current feedback signals. AC current reading range is 0mA to 10A and the device resolution is 0.1  $\mu$ A at 20 Hz readout. It has a RS-232 serial output via a null-modem connector.

#### **4.1.4. Oscilloscope**

Tektronix TDS 1002B, is a digital oscilloscope used for tracking the waveform changes in real time machining. It has a frequency range of 60 MHz and a sampling rate of 1 GS/s.

#### **4.1.5. Laser Displacement Sensor**

Keyence LK-G157, laser displacement sensor and LK-G3001V controller were used to precisely position the tool with respect to the work piece. Since it would be tedious to measure from the tip, the laser was shined on an extension plate sticking out of the tool electrode. The offset from the tip to the extended plate is measured under optical microscope each time a tip is inserted. Overall offset is subtracted from the reading to get the actual IEG. The resolution of the laser sensor is 0.5  $\mu$ m and the accuracy is within  $\pm 0.5\%$ . The sampling rate is 50 Khz. The laser sensor head and the controller are externally powered using a DC power supply 24 V.

Once the tool is positioned in a close proximity to workpiece in the machining range, the laser is no longer needed and the program can be started.

#### **4.1.6. Serial Interface Board**

Serial communication with the control computer was established using National Instruments PCI-8432/4 interface board. It has 4 serial I/O ports having 128 B transmit and receive. The board provides flexible baud rates for data transmissions between 57 b/s and 1 Mb/s to within 0.01% percent accuracy for standard baud rates.

### **4.2. SETUP**

#### **4.2.1. MicroECM Cell**

A microECM cell was designed and custom built. A Stainless steel tool holder can accept a different diameter electrodes. The holder is mounted at the end of the motor axis. The electrolyte is pumped through a hose and flushed from the tool tip. The fluid then recycled from the cell to the pump again, leaving sedimentary products at the bottom. *Figure 25* and *Figure 26* show designed schematic of the microECM cell and stepping actuator positioning and the actual microECM cell picture.

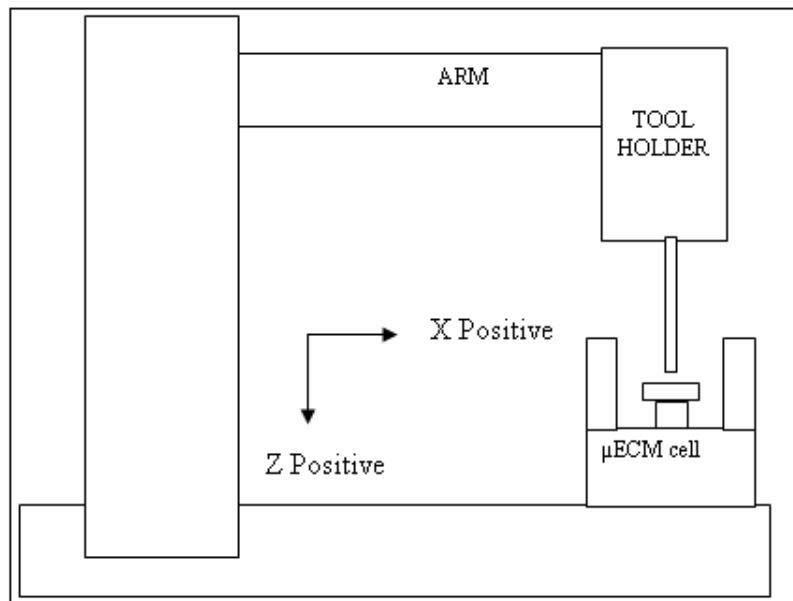


*Figure 25*  
**MicroECM cell with bi-slide actuator**



*Figure 26*  
**Custom built microECM cell**

Designed closed-loop microECM system was implemented. *Figure 27* shows the developed setup. A bidirectional manipulator using stepper motors was used as actuator mechanism. A 316L stainless steel pin,  $\text{Ø } 500 \text{ }\mu\text{m}$ , with ground and polished flat end, was rigidly clamped into a tool holder positioned above the microECM cell shown as item 7.

Environmentally friendly  $\text{NaNO}_3$  electrolyte was preferred over acidic solutions. The concentration was kept at 30g/l. The electrolyte was pumped and submerged tool electrode in a columnar flow.

The workpiece material was 0.5mm-thick 316L stainless steel plate. A function generator supplied the system with pulsed square wave in the range of 0.5-50 KHz. A digital oscilloscope provided online signal evaluation and an ammeter was used to monitor current change in the cell for feedback signal. An audio amplifier is employed to modulate the voltage amplitude. A high resolution laser displacement sensor was utilized to measure the displacement between the tool electrode workpiece. All the communications were provided using a serial communication board embedded in a computer.

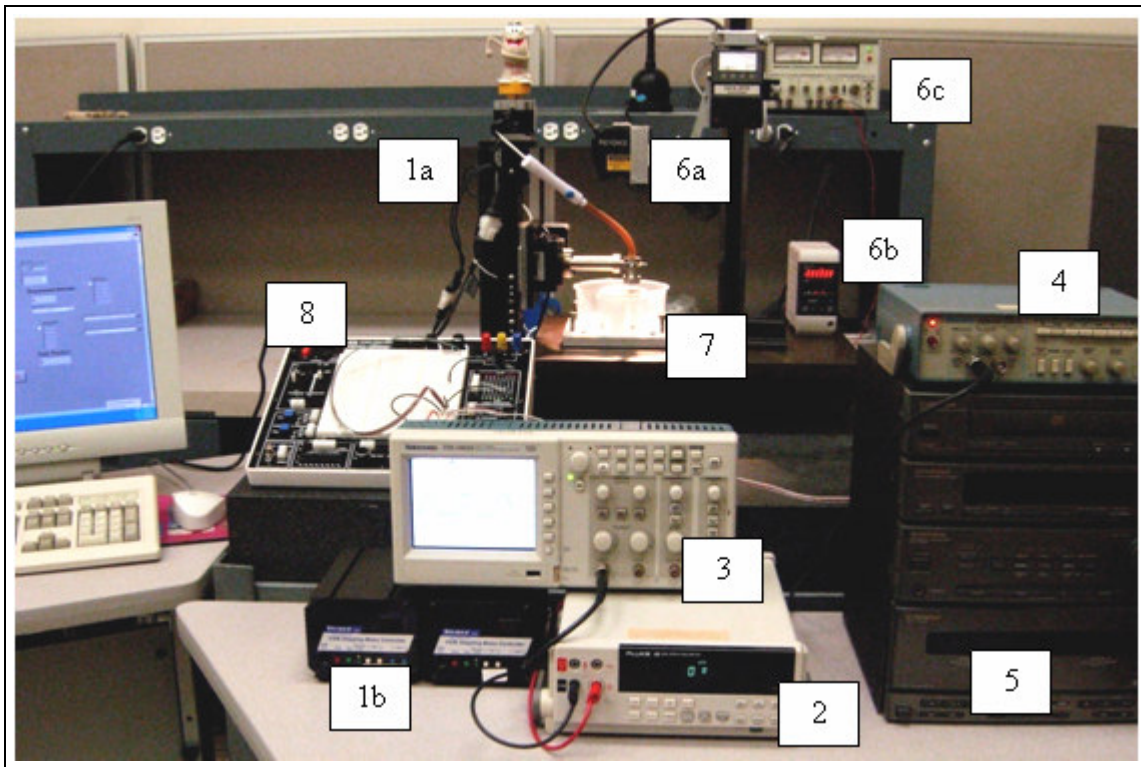


*Figure 27*

**Closed-loop microECM setup ((1a) stepper motors, (1b) motor controller, (2) ammeter, (3) oscilloscope, (4) function generator, (5) power amplifier, (6a) laser displacement sensor, (6b) lasercontroller and display, (6c) power source for laser unit, (7) microECM cell, (8) breadboard)**

## 4.3. EXPERIMENTS

### 4.3.1. Open-loop Experiments

Open-loop experiments were first tested by giving constant feed rate and displacement commands to stepper motor controllers. The objective for open-loop experiments is to form a basis for comparison with closed-loop experiments. Machined features were measured on an optical measuring microscope Olympus STM6 with 0.1  $\mu\text{m}$  resolution. The material removal rate was calculated from removed weight over time

and measured with Sartorius LE26P high precision weight balance, which has a resolution of 1 $\mu$ g. All open-loop experiments were run at a motor speed of 5  $\mu$ m/sec.

#### **4.3.2. Closed-loop Experiments**

Closed-loop experiments were carried out in a parametric method. The pulsed voltage amplitude was 16 V peak-to-peak (pp) with a minimum of -4 V and a maximum of 12 V for all experiments. The relatively small inverse polarity was required to promote the possible dissolution of plated product on the tool electrode during an inverse pulse. The pulse-on and pulse-off time ratio was kept at 1:1, which was long enough to dissipate heated electrolyte and produced gas.

##### **4.3.2.1. Dimensional Study**

Holes were machined for 60 seconds. A total of 70 holes were machined with 7 different frequencies, 5 repeats on both closed and open-loop systems. Same profiles were quantified for depth, diameter and MRR. Material removal also was observed increasing voltage supplied by a factor of 1.5 for specific set of variables. *Table 1* summarizes the parameters.

*Table 1*  
**Parameters for dimensional study experiments**

Electrode	Stainless steel pin, Ø 0.5 mm
Workpiece	Stainless steel (SS-316L), 0.5mm thick
Electrolyte	30 g/L sodium nitrate (NaNO <sub>3</sub> )
Frequency	0.5, 1, 2, 5, 10, 25, 50 KHz
Machining time	60 seconds
Voltage	16 Vpp (-4 V to 12 V) and 24 Vpp (-4 V to 20 V)
Pulse-on pulse-off ratio	1:1
Actuation mechanism	Open-loop, closed-loop

#### 4.3.2.2. Hysteresis Study

A separate set of experiments were realized for system hysteresis behavior. The depths were programmed to be 25  $\mu\text{m}$ , 50  $\mu\text{m}$ , 100  $\mu\text{m}$  and 200  $\mu\text{m}$  in forward and backward directions to note any hysterical variations. The experiments were repeated twice for both 0.5 KHz and 50 KHz frequencies. For the second set of experiments, tool electrode, workpiece, voltage and pulse-on pulse-off ratio was kept the same. *Table 2* shows parameter list for this set of experiments.



*Table 2*  
**Parameters for hysteresis study experiments**

Electrode	Stainless steel pin, Ø 0.5 mm
Workpiece	Stainless steel (SS-316L), 0.5mm thick
Electrolyte	30 g/L sodium nitrate (NaNO <sub>3</sub> )
Frequency	0.5 KHz, 50 KHz
Voltage	16 Vpp (-4 V to 12 V) and 24 Vpp (-4 V to 20 V)
Pulse-on pulse-off ratio	1:1
Actuation mechanism	Open-loop, closed-loop
Repeat	2
Direction	forward and backward
Hole depth	25, 50, 100 and 200 µm

## 5. RESULTS AND DISCUSSION

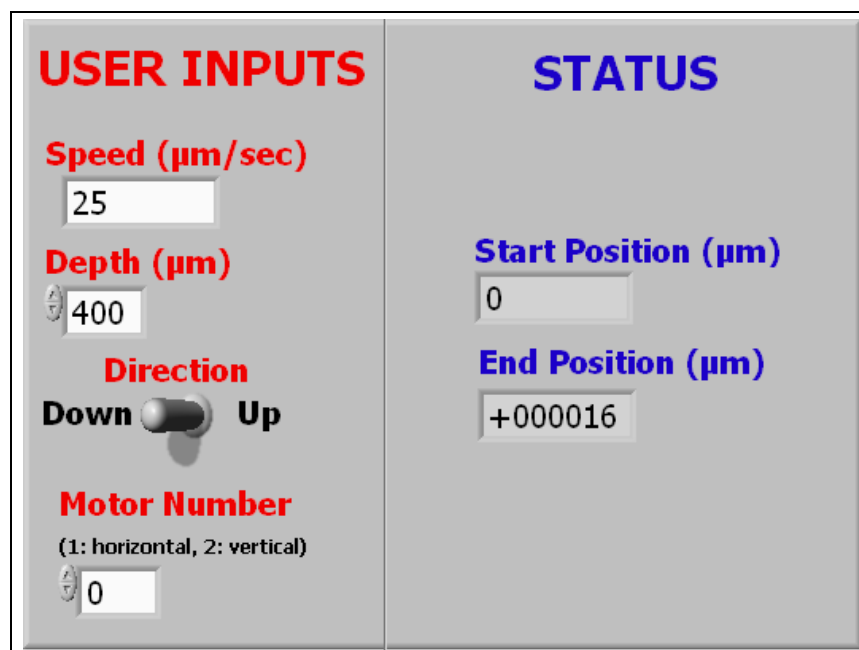
### 5.1. LABVIEW PROGRAMMING

Open-loop and closed-loop programs were developed using Labview 8.2.

Labview programming had the following advantages:

- Short initialization procedures
- Faster controlled experimentation
- Less variables in the system
- Control algorithms could be implemented



*Figure 28* shows developed open-loop interface front panel. Detailed explanation for the block diagrams and programming structure is provided in Appendix A.



*Figure 28*  
Open-loop Labview program front panel

Open-loop control has basic inputs as the depth, direction motor number to be actuated and speed. Since the system has no current feedback only position signal is retained in the memory for position data.

Closed-loop control program development is illustrated in *Figure 29*.

<b>PRIMARY USER INPUTS</b>		<b>SYSTEM STATUS</b>	
<b>Depth (<math>\mu\text{m}</math>)</b>		<b>Position (<math>\mu\text{m}</math>)</b>	
50		22.5	
<b>Direction</b>		<b>Current Density (<math>\text{mA}/\text{mm}^2</math>)</b>	
(up) <input type="radio"/> (down) <input checked="" type="radio"/>		315.24	
<b>Motor Number</b>		 	
(1:horizontal, 2:vertical)			
2			
<b>Step Magnitude (<math>\mu\text{m}</math>)</b>			
5			
<b>Proportional Gain</b>			
10			
<b>SECONDARY USER INPUTS</b>			
<b>Primary Multimeter Display</b> (0:AC current,5:Freq)		<b>Start Control Limit (<math>\text{mA}/\text{mm}^2</math>)</b>	<b>Step Wait (ms)</b>
AC Current 0		275	0
<b>Current Density Path</b>		<b>Lower Control Limit (<math>\text{mA}/\text{mm}^2</math>)</b>	<b>Upper Control Limit (<math>\text{mA}/\text{mm}^2</math>)</b>
C:\Current Density Values.txt		300	350
<b>Encoder Path</b>			
C:\Encoder Values.txt			

*Figure 29*  
**Closed-loop Labview program front panel**

Closed-loop control provides much more user access and flexibility. User enters target depth and defines speed by step magnitude and step wait times. Proportional constant is required for the particular case when the program starts on a random position where no current data is initially present. Then, the tool would be forwarded to the workpiece faster, with a rate defined by P constant. The detail on the closed-loop block diagram and programming is given in Appendix B.

For saving and recording purposes, the spontaneous current readings and motor position readings can be saved to a text file for ease of plotting or post-experimental analysis. Example machining process is plotted in *Figure 30*.

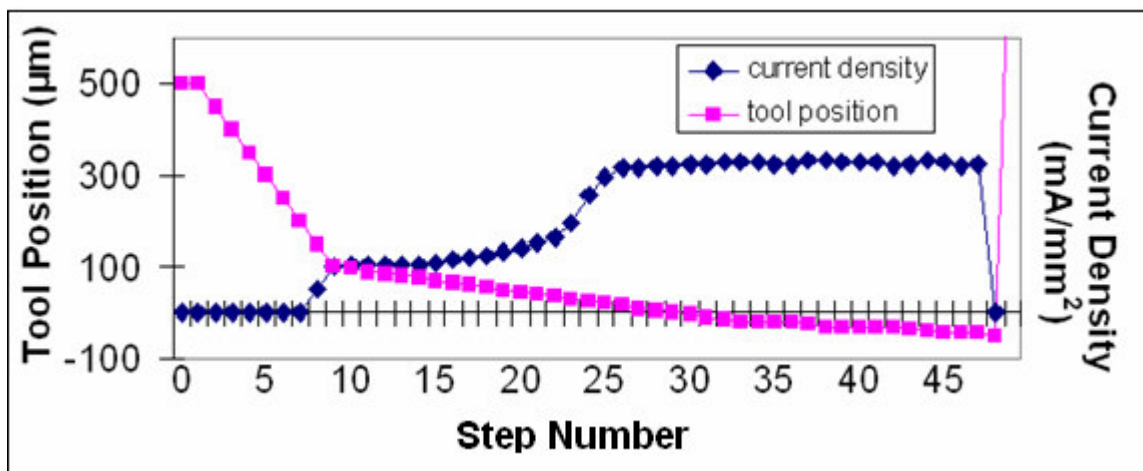


*Figure 30*

**An example machining process (50 steps , 16 Vpp, 30 g/L NaNO<sub>3</sub>, 500 Hz, Ø 0.5mm electrode)**

Machining set limit conditions also should be defined initially since the program would compute the current density reading and compare with the presets. For this purpose an initial open-loop run was necessary to calibrate the current density-IEG

relationship. The calibration curve is plotted in *Figure 31*. The current values were normalized to current densities by including area of tool electrode. Drastic drop of current density was seen at IEG about 20  $\mu\text{m}$ . Therefore, the machining current density limits were determined to be on an effective range from 300-350  $\text{mA}/\text{mm}^2$ . The control algorithm upper and lower limits were set to be on this range. The start limit is set to be 275  $\text{mA}/\text{mm}^2$  for the particular parameters since current density loses its meaning below that value corresponding larger IEG.

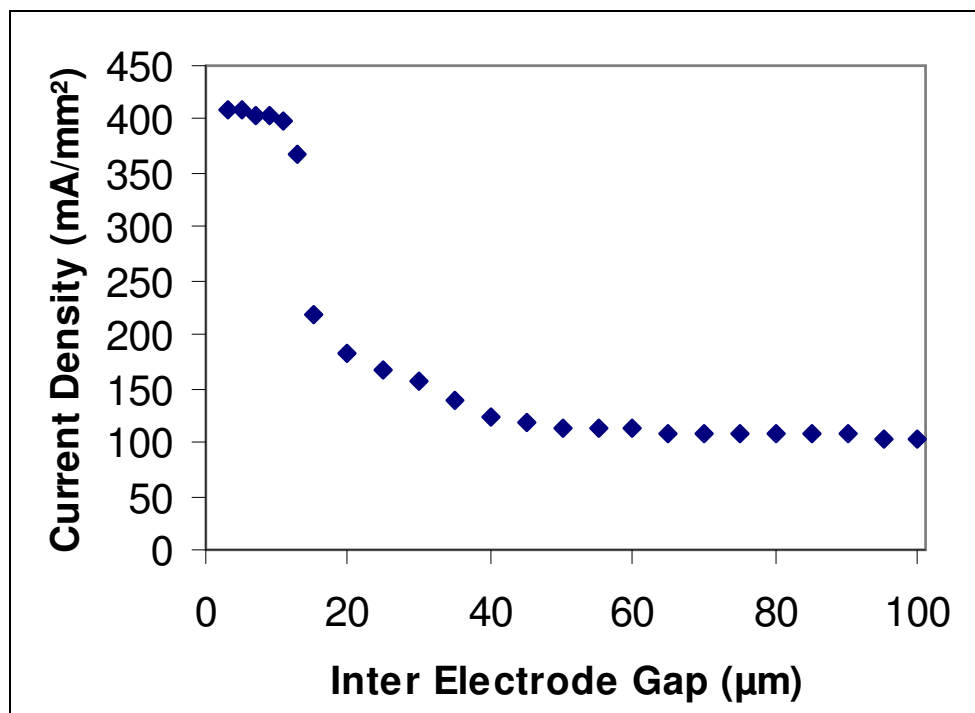


*Figure 31*

**Effect of electrode gap on ECM current density (316L ss, 30 g/L  $\text{NaNO}_3$ , 500 Hz, 16 V pp,  $\varnothing$  0.5 mm electrode)**

## 5.2. EFFECT OF FREQUENCY ON THE HOLE DEPTH AND DIAMETER

Hole diameter and hole depth versus frequency are plotted in *Figure 32* and *Figure 33* respectively. Quantitative decrease in the both features was noticed with increasing frequency and agreed with previous works (Kenney and Hwang 2005). It was observed that open-loop system creates bigger hole openings on the surface since there was an uncertain time spent in between machining steps using constant velocity, bringing an undesired size increase on the orifice and introduce a non-uniform hole profile along the depth. The uncertainty can also be seen by noticing on the size variations. On the other hand the closed-loop system was remarkably better in achieving deeper profiles. The controlled tool speed and displacement increased the efficiency in reaching much higher aspect ratios when combined with the smaller diameter holes. The closed-loop system proved to be repeatable and it was seen in low variation values on plots.

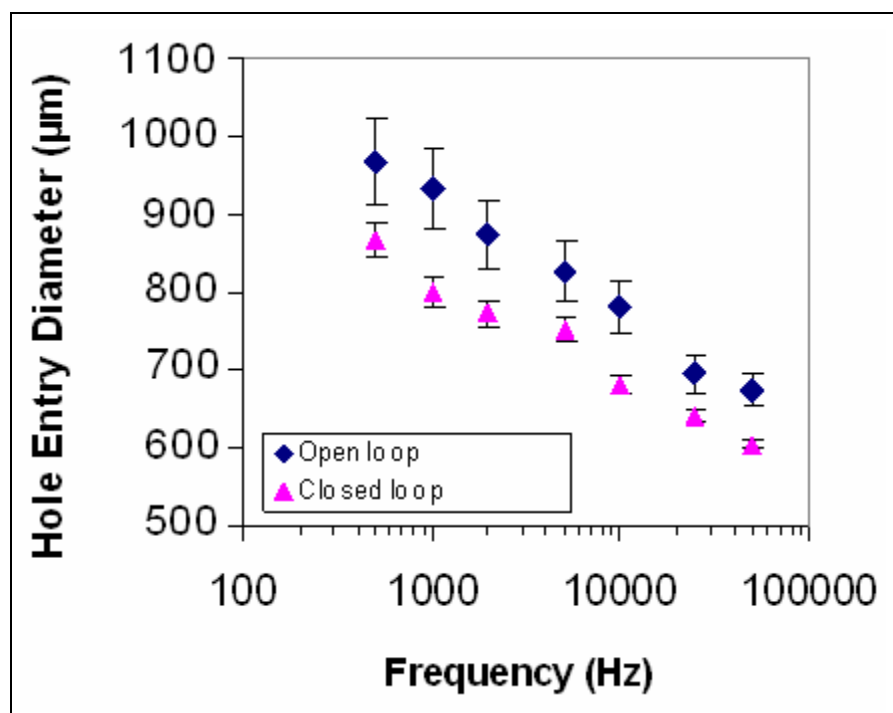


*Figure 32*

**Effect of frequency on hole diameter (316L ss, 30 g/L NaNO<sub>3</sub>, 16 V pp, Ø 0.5 mm electrode)**

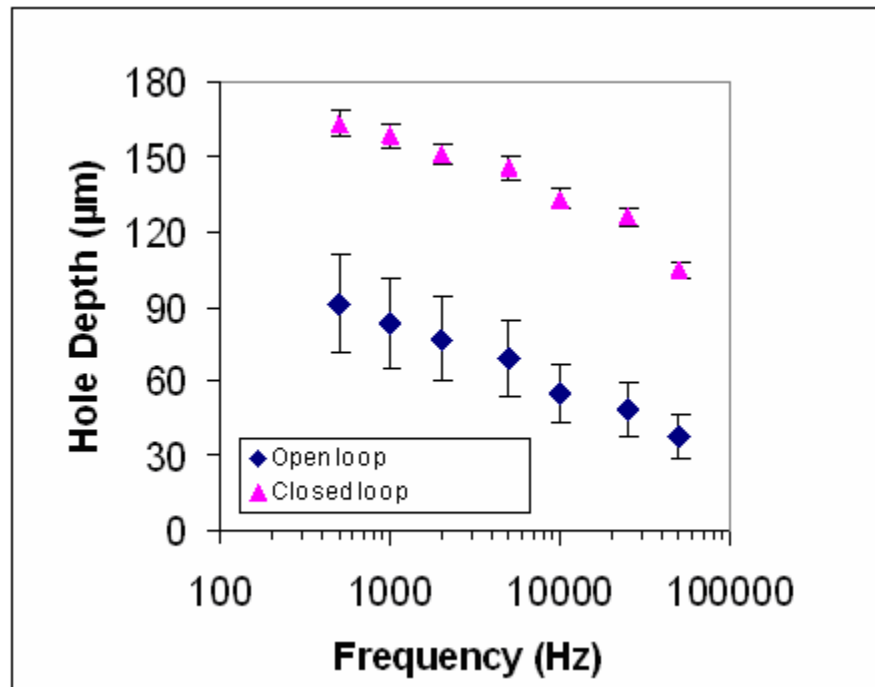


*Figure 33*  
**Effect of frequency on hole depth (316L ss, 30 g/L NaNO<sub>3</sub>, 16 V pp, Ø 0.5 mm electrode)**

*Figure 34* shows the MRR by theory and open-loop and closed-loop experiments. The theoretical value of removal volume is calculated using equation (8). Feedback controlled closed-loop system had a significant advantage due to the deeper hole profiles and less amount of machining time spent as a result of both velocity and displacement control. Closed-loop machining MRR converged to the theoretical values by an increase of 250% on open-loop machining. The repeatability was most obvious in MRR experiments since even a small time loss has a dramatic effect on a relatively short machining time of one minute. The average variation in MRR was reduced by 88% in closed-loop machining.



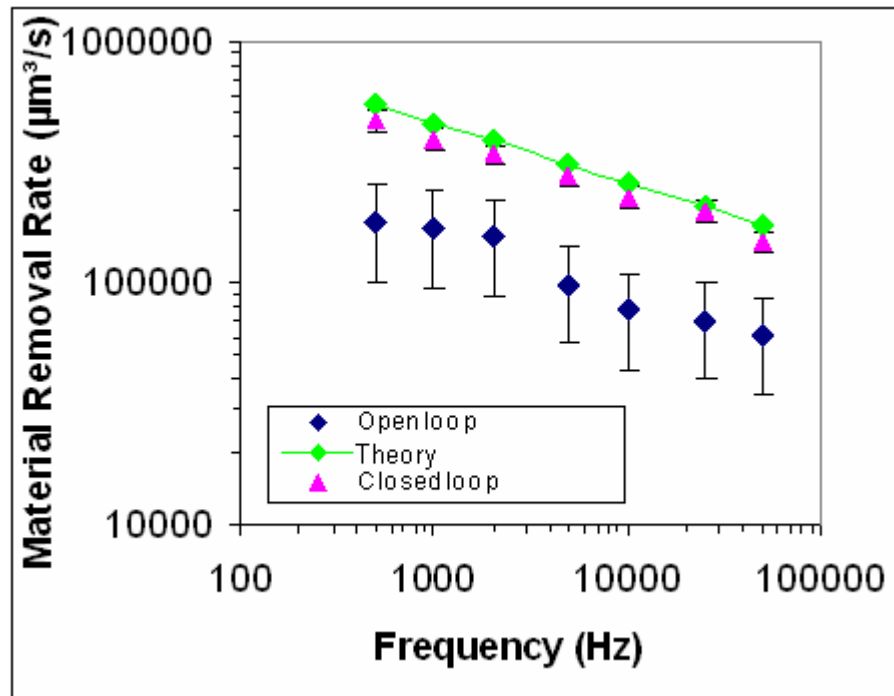
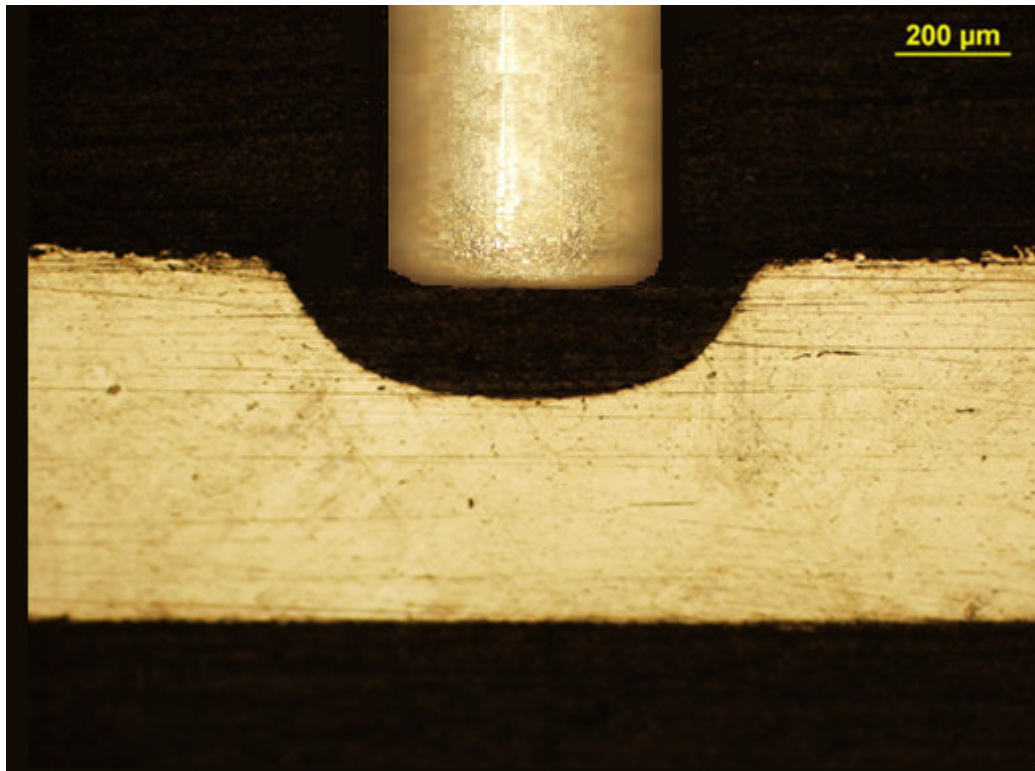


Figure 34

Material removal rate with frequency (316L ss, 30 g/L NaNO<sub>3</sub>, 16 V pp, Ø 0.5 mm electrode)

### 5.3. HOLE PROFILE

By utilizing the closed-loop control, we investigated the entry/exit hole uniformity, variations and enhancements over open-loop system by drilling through holes. *Figure 35* shows a cross sectional view of the tool-hole superposition. The tapered side wall profile is due to the nature of current density distribution from the tool side walls as the tip advances into the workpiece. However, in open-loop systems excessive machining time loss yields a large, bowl-like opening for the holes. This causes unwanted surface damage and increased aspect ratio.



*Figure 35*  
**Cross sectional tool electrode and machined hole**

The uncertain waiting time was eliminated using closed-loop system. This way, the tool was not lingered above the workpiece surface and forwarded into the material subsequent the current feedback. The resulting optical images are given in *Figure 36*. The open-loop hole had a large surface damage causing a very large initial diameter, whereas closed-loop entry hole had significantly less damaged surface and machining tool place on the desired region. Quality of the hole profile, hence increased, having sharper edges with smaller curvature radius at the opening. Higher aspect ratio features could be obtained using closed-loop system. Undesired surface damage decreased 97% due to closed-loop controlled machining.

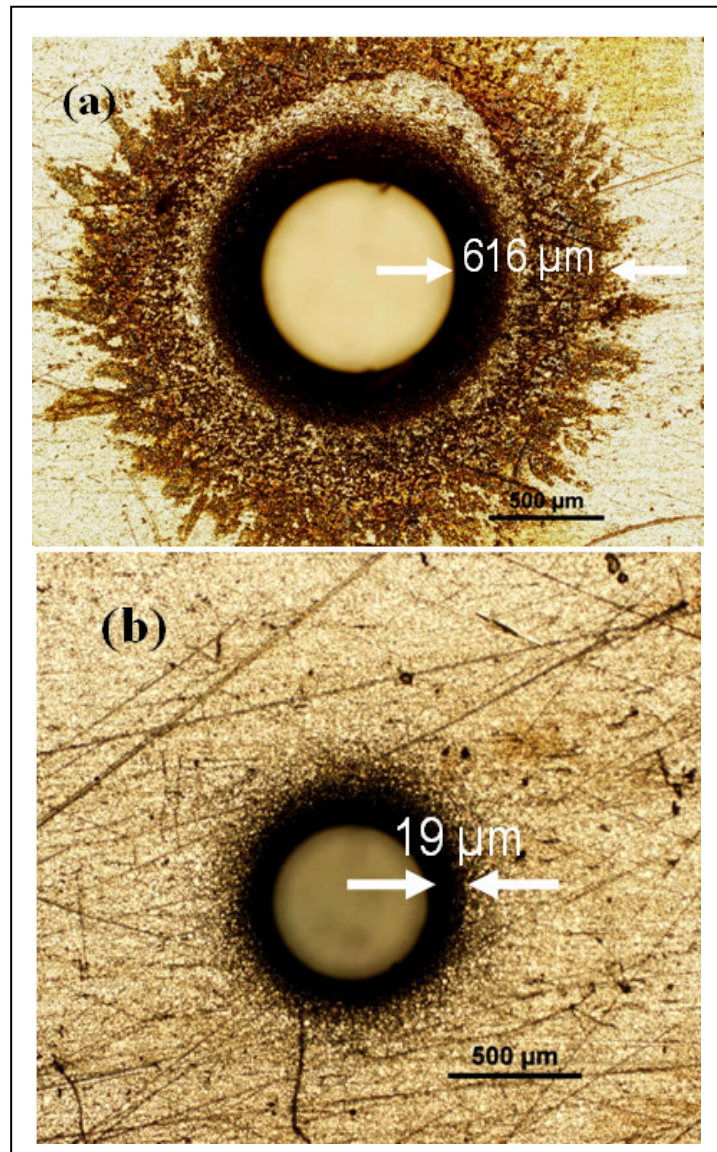


*Figure 36*

**MicroECM hole profile images (top view of entry hole after ECM'ing with (a) open loop control and (b) closed-loop control) (316L ss, 30 g/L NaNO<sub>3</sub>, 50 KHz, 16V pp)**

#### 5.4. SYSTEM HYSTERESIS

System hysteresis gives quantitative information on variability and repeatability of the system. The hysteresis on programmed and measured hole depths is shown in *Figure 37*. No hysteresis was observed and high conciliation of programmed and measured hole depth was established at both low and high frequencies. Perfect hysteresis is not expected for travel distances less than the stepper resolution (2.5  $\mu\text{m}$ ). Also at higher frequencies machining side and front gap decreases, which converges the linear fit to zero intercept. This finding is agreed with the well established microECM dynamics (Kenney and Hwang 2005).

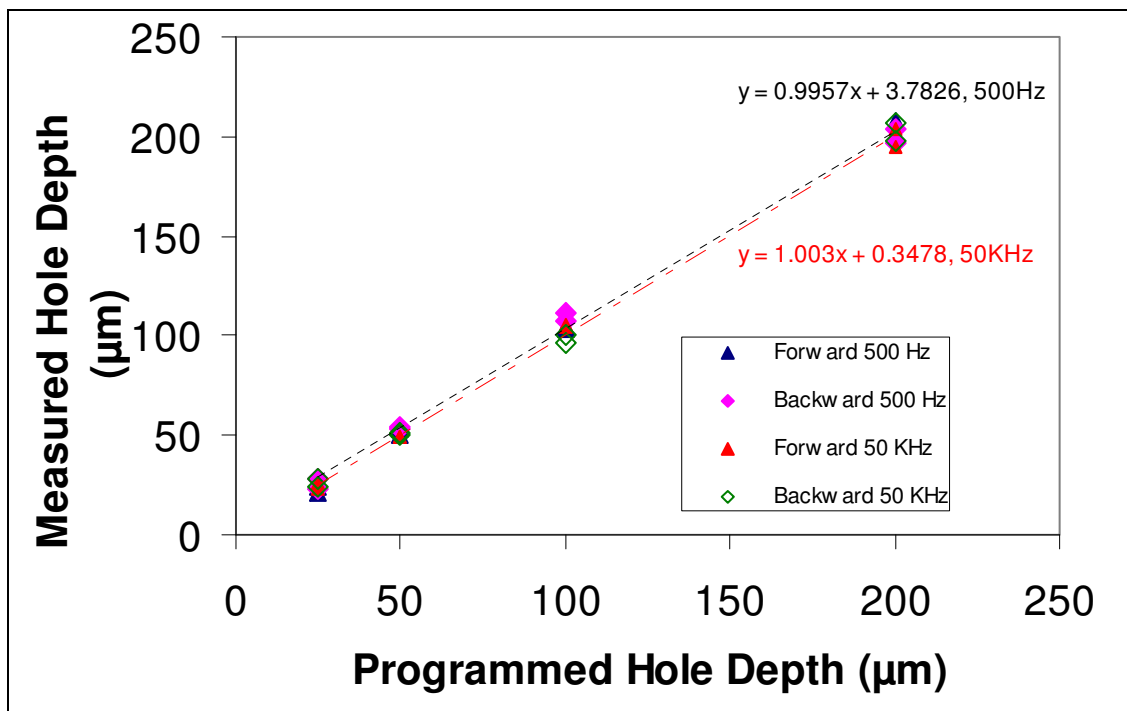


*Figure 37*  
Hysteresis study (316L ss, 30 g/L NaNO<sub>3</sub>, 0.5-50 KHz, 16 V pp)

### 5.5. EFFECT OF AMPLIFICATION

The effect of amplification was investigated. Regular 16 Vpp was amplified by an amplification ratio of 1.5 and brought to 24 Vpp. Closed-loop system was used and a random parameter combination was tested over 60 seconds machining. Amplification effect is shown in *Figure 38*. Amplification effect is compared with the theoretical MRR. The closed-loop system exhibits little difference with the theory and MRR was increased approximately 1.5 times with an amplification ratio of 1.5.

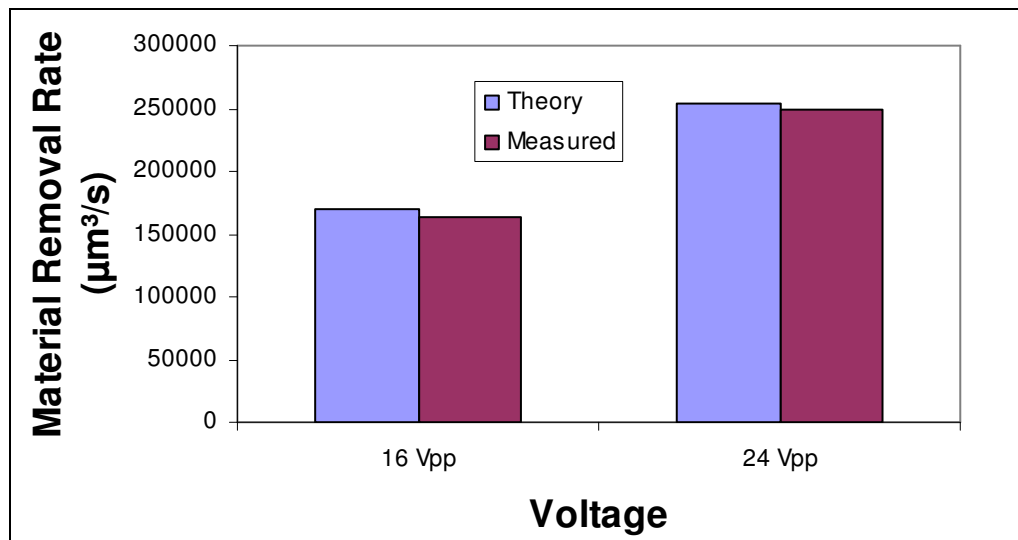


*Figure 38*  
Effect of amplification (316L ss, 30 g/L NaNO<sub>3</sub>, 50 KHz, 16-24 Vpp)

## 6. CONCLUSIONS & RECOMMENDATIONS

A microECM system with closed-loop control was developed. It was found that:

- 1) High frequency pulsed input reduced feature size and material removal rate but improved feature quality. Closed-loop tool position and velocity control provides faster machining time and higher material removal rate.
- 2) Binary algorithms were applied to certain machining scenarios to take measures and manipulate output. Binary control logic was suitable for the stepper motor system and parametric conditions. Position and velocity control is established for increased material removal rate and overall feature quality.
- 3) The material removal rate was increased by 250% on closed-loop system compared to open loop system since undesired time loss due to undesired larger IEG machining is prevented. MRR was found to be very close to theory in closed-loop system whereas, it was significantly lower in open-loop setup. Machining variation is significantly reduced, by 88% on microfeatures. Hole quality and sharpness is increased by 97%. Only target zone was machined due to the system localized dynamics and unwanted surface damage was averted.
- 4) Electrode gap can be reduced within the machining limits to a smaller distance, where more effective machining is possible. Repeatable machining with much less variations compared to open-loop system is also a characteristic of the automated closed-loop microECM.
- 5) The advantages of the feedback controlled closed-loop microECM can be listed,

- Faster machining with higher removal rates
- Repeatable, less varied machined features
- Better surface finish since tool contact short circuiting is avoided.

For future study:

- 1) The microECM system can be improved by providing real time control of pulse amplitude from the power supply in addition to current control. This requires enhanced control algorithms and since dynamic power supply introduces another dimension to the system.
- 2) A lookup table can be established, where specific lower, upper and start limits for current density values could be automatically set, depending on the voltage applied, workpiece material, tool diameter and frequency. Thus, there would not be need for any calibration curve for particular experiments.
- 3) Position control can become automatic by providing an additional feedback loop from the laser displacement sensor. Voltage reading can be traced out of the analog output of the laser controller and acquired using a data acquisition board.

## REFERENCES

- Amalnik, M.S. and McGeough J.A. (1996). "Intelligent concurrent manufacturability evaluation of design for electrochemical machining." *Journal of Material Processing Technology* (v61, n1), pp130-139.
- Bard, A.J. and Faulkner, L. R. (1980). *Electrochemical Methods: Fundamentals and Applications*. New York: John Wiley & Sons, Inc.
- Bejar, M.A. and Eterovich, F. (1995). "Wire-electrochemical cutting with  $\text{NaNO}_3$  electrolyte." *Journal of Materials Processing Technology* (v55, n3), pp417-420.
- Benedict, G. F. (1987) *Nontraditional Manufacturing Processes*. Boca Raton, FL: CRC Press, pp133.
- Bhattacharyya, B. and Munda, J. (2003). "Experimental investigation on the influence of electrochemical machining parameters on machining rate and accuracy in micromachining domain." *International Journal of Machine Tools and Manufacture* (v43, n13), pp1301-1310.
- Bhattacharyya, B., Malapati, M. and Munda, J. (2005). "Experimental study on electrochemical micromachining." *Journal of Materials Processing Technology* (v169, n3), pp485-492.
- Bhattacharyya, B., Munda, J. and Malapati, M. (2005). "Advancement in electrochemical micro-machining." *International Journal of Machine Tools and Manufacture* (v44, n15), pp1577-1589.
- Brogan, W.L. (1985). *Modern Control Theory*. Upper Saddle River, NJ: Prentice Hall.
- Cagnon, L., Kirchner, V., Kock, M., Schuster, R., Ertl, G., Gmelin, W.T. and Kück, H. (2003). "Electrochemical micromachining of stainless steel by ultrashort voltage pulses." *Zeitschrift für Physikalische Chemie* (v217, n4), pp299-313.
- Chikamori, K. (1998). "Possibilities of electrochemical micromachining." *International Journal of the Japan Society for Precision Engineering* (v32, n1), pp-37-38.
- Dabrowski, L. and Paczkowski T. (2005). "Computer simulation of two-dimensional electrolyte flow in electrochemical machining." *Russian Journal of Electrochemistry* (v41, n1), pp91-98.



- Datta, M. (1995). "Fabrication of an array of precision nozzles by through-mask electrochemical micromachining." *Journal of the Electrochemical Society* (v142, n11), pp3801-3805.
- Datta, M. (1998). "Microfabrication by electrochemical metal removal." *IBM Journal of Research and Development* (v42, n5), pp655-669.
- Davydov, A.D., Volgin, V.M. and Lyubimov, V.V. (2004). "Electrochemical machining of metals: fundamentals of electrochemical shaping." *Russian Journal of Electrochemistry* (v40, n12), pp1230-1265.
- De Silva, A.K.M. and McGeough J.A. (1998). "Process monitoring of electrochemical micromachining." *Journal of Materials Processing Technology* (v76, n1-3), pp165-169.
- Dorf, R. C. (1992). *Modern Control Systems, 6<sup>th</sup> ed.* Reading, MA: Addison-Wesley Publishing Company, Inc.
- Förster, R., Scoth, A. and Menz, W. (2005). "Micro-ECM for production of Microsystems with high aspect ratio." *Microsystem Technologies* (v11, n4-5), pp246-249.
- Jain, V.K. and Rajurkar, K.P. (1991). "An integrated approach for tool design in ECM." *Precision Engineering* (v13, n2), pp111-124.
- Jerman H. and Terry S. (1997). *Microlithography, Micromachining & Microfabrication, vol. 2.* Bellingham, WA: SPIE Optical Engineering Press, pp379-434.
- Kenney, J.A. and Hwang, G.S. (2005). "Electrochemical machining with ultrashort voltage pulses: modelling of charging dynamics and feature profile evolution." *Nanotechnology* (v16, n7), ppS309-S313.
- Kirchner, V., Cagnon, L., Schuster, R. and Ertl, G. (2001). "Electrochemical machining of stainless steel microelements with ultrashort voltage pulses." *Applied Physics Letters* (v79, n11), pp1721-1723.
- Kozak, J., Rajurkar K.P. and Wei, B. (1994). "Modeling and analysis of pulse electrochemical machining (PECM)." *Trans. of the ASME* (v116, n3), pp316-323.
- Lee, E.S., Baek, S.Y. and Cho, C.R. (2007). "A study of the characteristics for electrochemical micromachining with ultrashort voltage pulses." *The International Journal of Advanced Manufacturing Technology* (v31, n7-8), pp762-769.

- Maeda, R., Chikamori, K. and Yamamoto, H. (1984). "Feed rate of wire electrochemical machining using pulsed current." *Precision Engineering* (v6, n4), pp193-199.
- Mukherjee, S.K., Kumar, S. and Srivastava, P.K. (2005). "Effect of over voltage on material removal rate during electrochemical machining." *Tamkang Journal of Science and Engineering* (v8, n1), pp23-28.
- Ogata, K. (1997). *Modern Control Engineering*. Upper Saddle River, NJ: Prentice-Hall, pp212.
- Osenbrugger, C. and Regt, C. (1985). "Electrochemical micromachining." *Philips Technical Review* (v42), pp22-32.
- Park, B.J., Kim, B.H. and Chu, C.N. (2006). "The effects of tool electrode size on characteristics of micro electrochemical machining." *Annals of the CIRP* (v55, n1), pp197-200.
- Park, M.S. and Chu, C. N. (2007). "Micro-electrochemical machining using multiple tool electrodes." *Journal of Micromechanics and Microengineering* (v17, n8), pp1451-1457.
- Rai-Coudhury P., Ed. (1997). *Handbook of Microlithography, Micromachining & Microfabrication*. Bellingham, WA: SPIE Optical Engineering Press.
- Rajurkar, K.P., Zhu, D., McGeough, J.A., Kozak, J. and De Silva, A. (1999). "New developments in electrochemical machining." *Annals of the CIRP* (v48, n2), pp567-580.
- Santini, J. T., Cima, M. J. and Langer, R. (1999). "A controlled release microchip." *Nature* (v397, n6717), pp335-338.
- Sen, M. and Shan, H.S. (2003). "Comparative study of small hole drilling in Nimonic C-263." *Proc. of the 13<sup>th</sup> ISME Conference, Roorkee, India PE-033*.
- Schuster, R., Kirchner, V., Allongue, P. and Ertl, G. (2000). "Electrochemical micromachining." *Science* (v289, n5476), pp98-101.
- Skrabalak, G., Skrabalak, M.Z. and Ruszaj, A. (2004). "Building of rules base for fuzzy-logic control of the ECDM process." *Journal of Materials Processing Technology* (v149, n1-3), pp530-535.
- Tehrani A.F. and Atkinson J. (2000). "Overcut in pulsed electrochemical grinding." *Proc. of the Institution of Mechanical Engineers, Part B Journal of Engineering Manufacture* (v24, n4), pp259-269.

Uhlmann, E., Doll, U., Forster, R. and Schikofsky, R. (2001). "High precision manufacturing using PEM." *Proc. of the International Symposium for Electromachining (ISEM XIII)*, Bilbao, Spain (v1), pp261-268.

Vectron Deburring (2006). <http://www.vectron.cc/photo1.html>.

Yong, L., Yunfei, Z., Guang, Y. and Liangqiang, P. (2003). "Localized electrochemical micromachining with gap control." *Sensors and Actuators A* (v108, n1), pp144-148.

Zhang, Z., Zhu, D., Qu, N. and Wang, M. (2007). "Theoretical and experimental investigation on electrochemical micromachining." *Microsystem Technologies* (v13, n7), pp607-612.

Zhou, C.D., Taylor, E.J., Sun, J.J., Gebralt, L., Stortz, E.C. and Renz, R.P. (1997). "Electrochemical machining of hard passive alloys with pulse reverse current." *Trans. NAMRI/SME* (v25), pp147-152.

## APPENDIX A

### OPEN-LOOP CONTROL VISUAL INSTRUMENT PROGRAMMING

An open-loop control visual instrument (VI) code was programmed in National Instruments Labview version 8.2. Labview programs consist of two major sections:

- Front panel
- Block diagrams

Front panel is the interface where all the control and indicator graphics take place. This is basically the panel the user is watching, entering inputs and starting/stopping the program. Front panel is the highest level in VI programming.

Block diagrams are actual codes that run the program and they are in back stage. The user is not interested with the code once the program is ready for execution. All block diagrams are related to front panel objects. Block diagrams are lower level in VI programming. Block diagram for open-loop control is given in *Figure A-1*.

Actuation commands are sent to motor controller in a string format. Velmex, VXM controller accepts the commands only in this format. Commands used in this study are given below:

ImMx: set steps incremental (m: motor number, x: distance from 1 to 16,777,215.

SmMx: set speed of motor (m: motor number, x: speed from 1 to 6000 steps/sec.

PM-x: select and clear all commands from program number x.

C: clear all commands from currently selected program.

R: run currently selected program.

Q: quit online mode.

F : enable online mode with echo off.

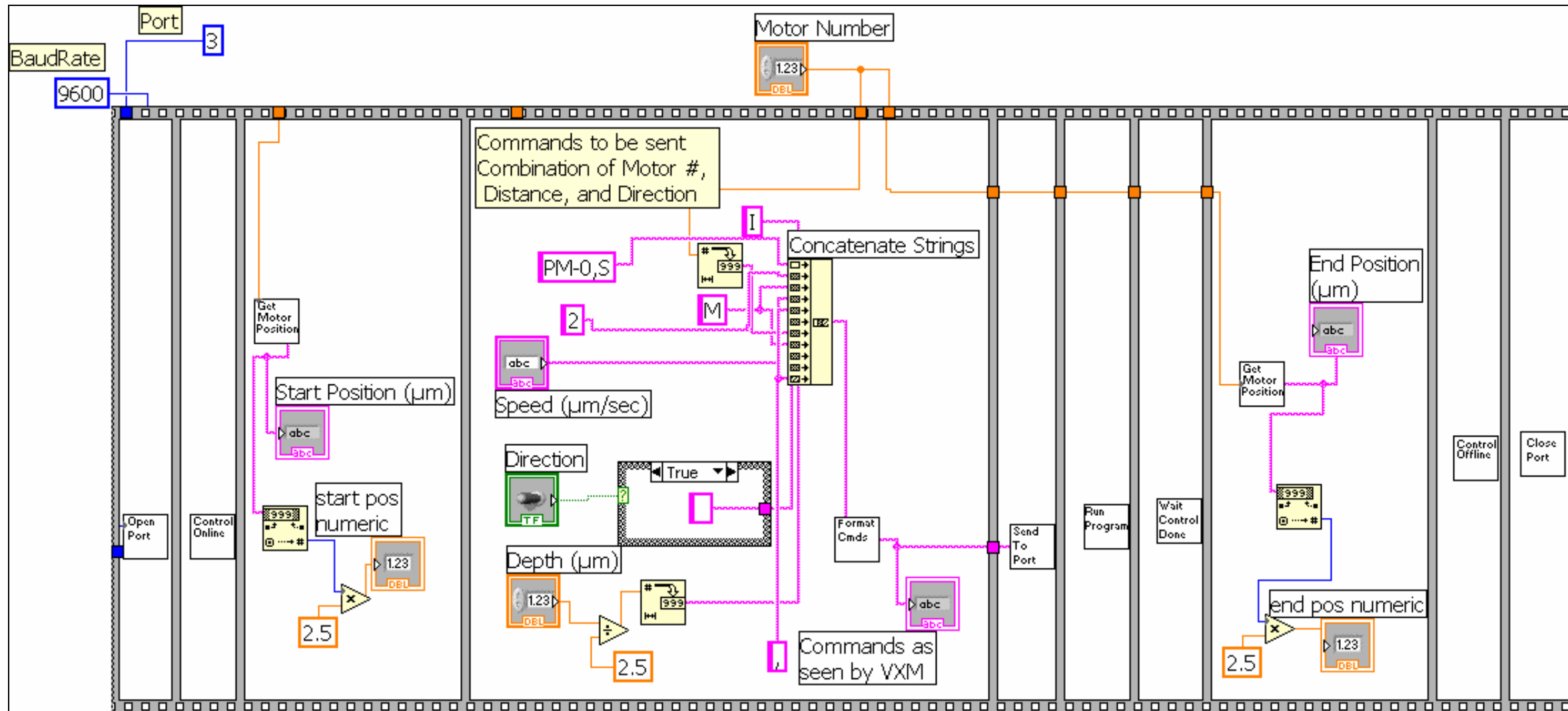


Figure A-1  
Open-loop control Labview block diagram

*Figure A-1* consists of several windows positioned side by side. Once the operation in previous window is executed, the operation in the next window at the right side is ready for execution. This sort of sequence is called flat sequence. The execution steps are as follows:

1) In the first window at leftmost side, the ports are opened and constant baud rate is determined to start serial programming. The open port box is treated as a black box and is the stepping motor instrument driver property.

2) The control is brought to online, so the computer is ready to communicate with the device.

3) Previous motor position is recorded through the step count and written in start position indicator box. Steps are converted to micrometer distance, since the stepping motor has a resolution of  $2.5 \mu\text{m}/\text{steps}$ .

4) Input motor number is recorded for the actuation direction. Depth and speed values are recorded into memory buffer and the string is concatenated before sending to stepping motor controller. Depth step input is externally converted to a string value in micrometer unit.

5) Commands are sent to port.

6) Program run.

7) Controller is done communicating the device.

8) End motor position is recorded and converted to micrometer distance unit.

9) Controller is offline.

10) Ports are closed.

## APPENDIX B

### CLOSED-LOOP CONTROL VISUAL INSTRUMENT PROGRAMMING

Closed-loop control VI programming is more involved taking number of instruments and actuation, sensing mechanisms into consideration. The block diagrams are formed in the form of stacked sequence. Contrary to flat sequence, in stacked sequence the windows are separated. However, the execution method is again sequential; program execution for the next window requires the termination of program execution for the previous window.

The publicly available drivers for both Velmex VXM controller and Fluke 45 ammeter have been utilized and developed for closed-loop controlled actuation and sensing.

There are 9 stacked sequence and they are described in the following:

#### **Sequence 0**

Initial zero sequence simply opens VXM stepper motor driver port making the device ready for communicating the media connected. *Figure B-1* shows initialization sequence.



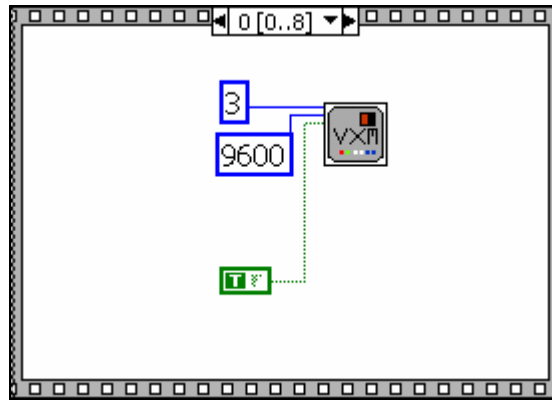


*Figure B-1*  
**Sequence 0**

### **Sequence 1**

First sequence brings the VXM stepper motor controller driver online. This step is shown in *Figure B-2*.

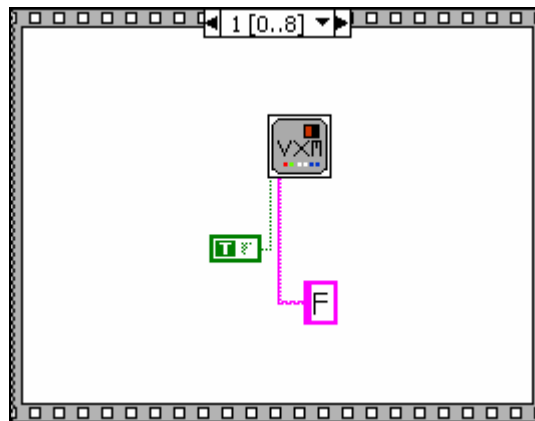


*Figure B-2*  
**Sequence 1**

## Sequence 2

Second sequence initialize the Fluke 45 ammeter. This initialization is done once and references with arrows. However current reading is kept in a loop and shown in the next sequences. This step is shown in *Figure B-3*.

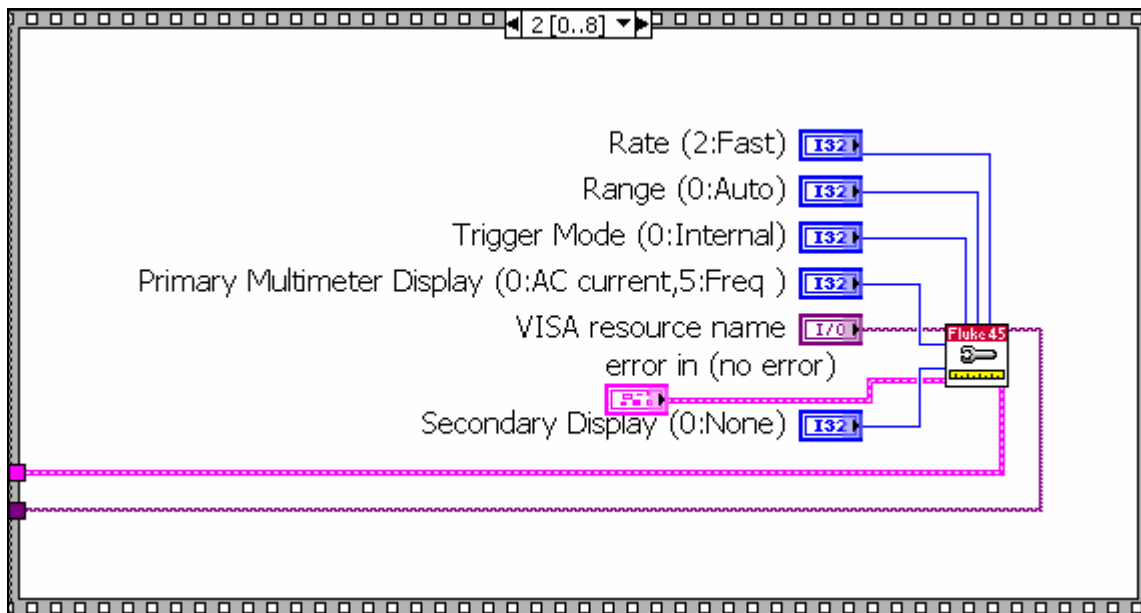


*Figure B-3*  
**Sequence 2**

## Sequence 3

Third sequence is used for getting the position data, so the program lets user know of the current motor position. Motor number is referenced from the user input in the next sequence. String values are converted to numeric values using a labview converter. Steps are converted to micrometers by simply multiplying by 2.5. A negative sign is necessary since the downward direction of motors is taken as positive direction.

Sequence is depicted in *Figure B-4*.

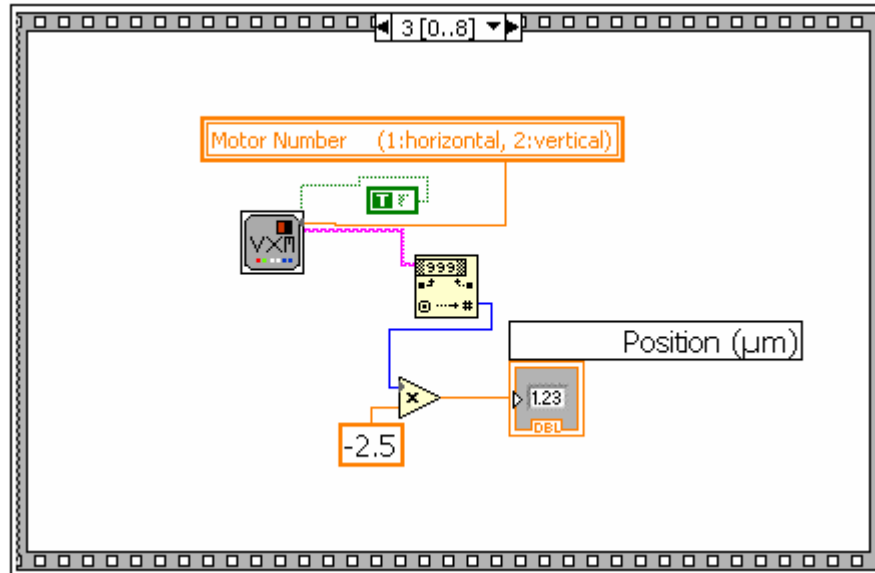


*Figure B-4*  
**Sequence 3**

#### Sequence 4

Since case structure and true false conditions are introduced here, the subsequences and conditions are explained separately.

##### 4.1.

At sequence 4.1, current density for start control limit is checked. If the tool is far away from the workpiece, then no current density will be read so the tool should be advanced toward the workpiece faster by proportional control. *Figure B-5* introduces the case structure. It is a true/false check for a given case. The false statement means in that particular case that the assumption of system current density being lower than the user

input start limit is false. So, the current density is not below the user input low limit.

Therefore the system terminates the check loop and goes for sequence 5.

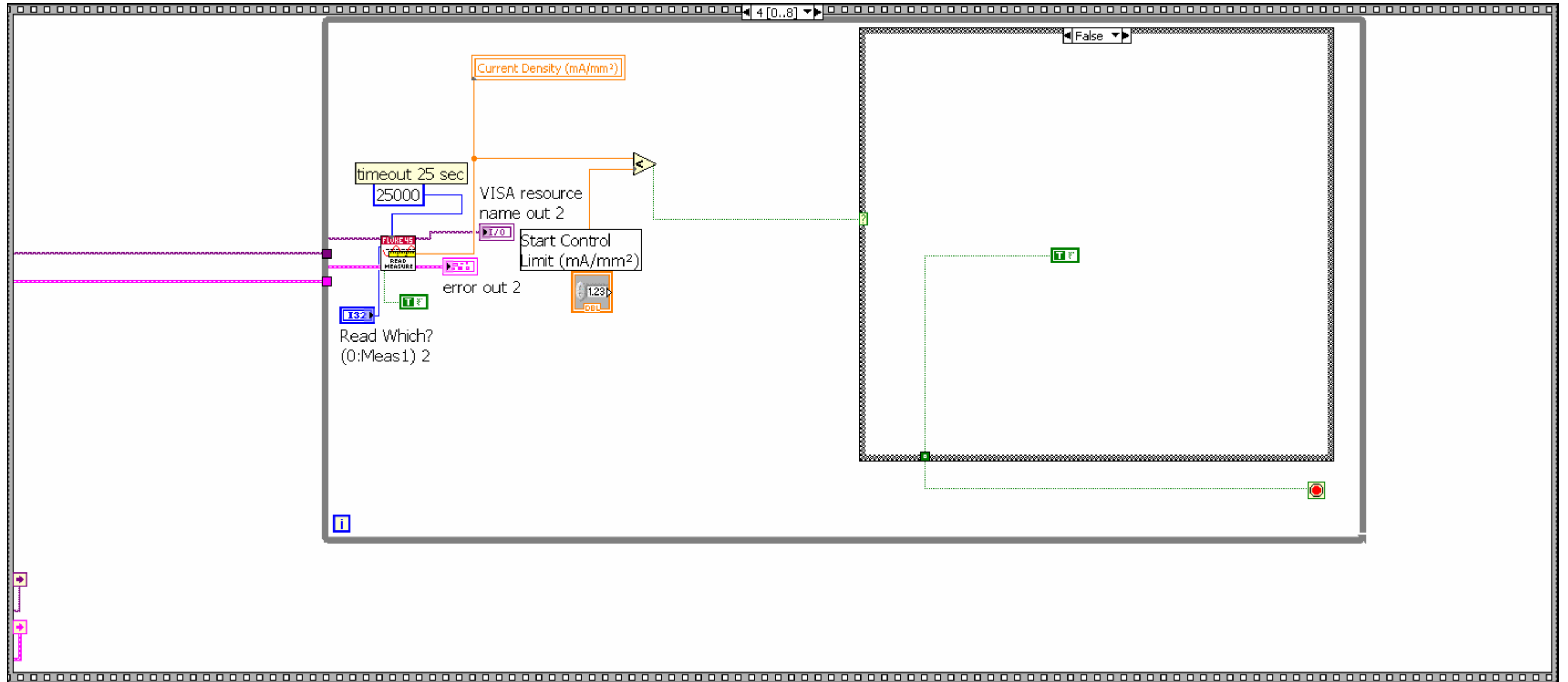


Figure B-5  
Sequence 4,1

**4.2.**

Following the sequence 4.1, at sequence 4.2, the true condition is computerized. If the condition is true, then the tool is rushed towards workpiece by a velocity defined by user input P constant. Step magnitude is the distance the stepping motor should go in one execution command. Since the stepping motor is not continuously interrupted, step size is an important parameter. Step magnitude is then multiplied by proportional constant for a larger step size, hence higher speed. The step is illustrated in *Figure B-6*.

**4.3-4.**

Following this check, program run and position recording steps are illustrated in *Figure B-7* and *Figure B-8* respectively. For space convenience, the current density check portion of the table is omitted and conditional portion is given. Program is ran by sending an R string command to the controller. Position is again recorded after a step/micrometer conversion.

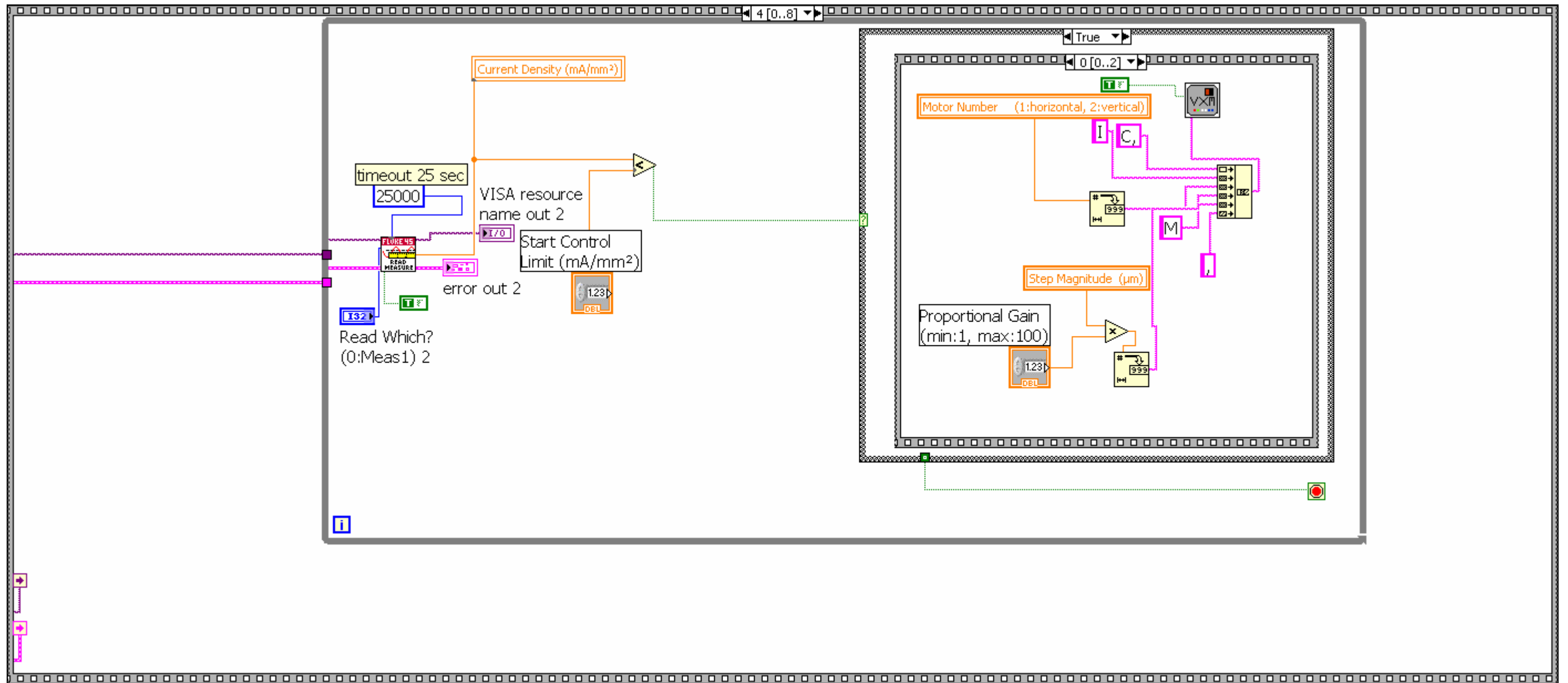
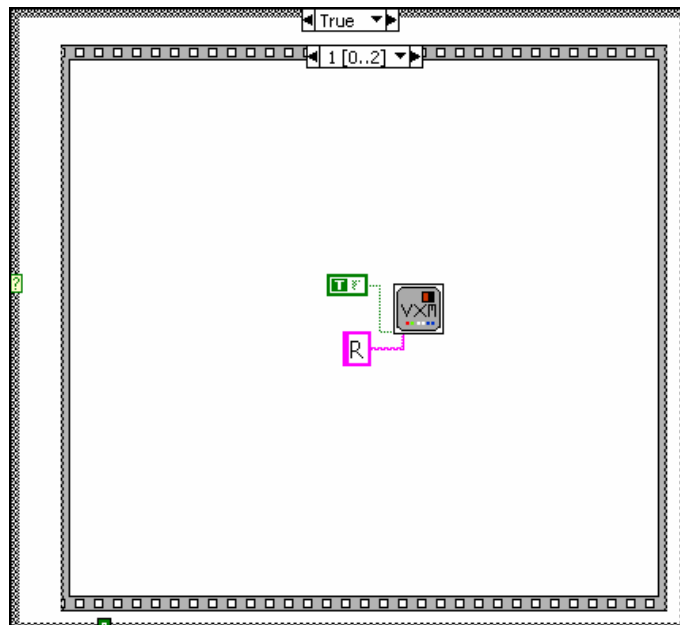
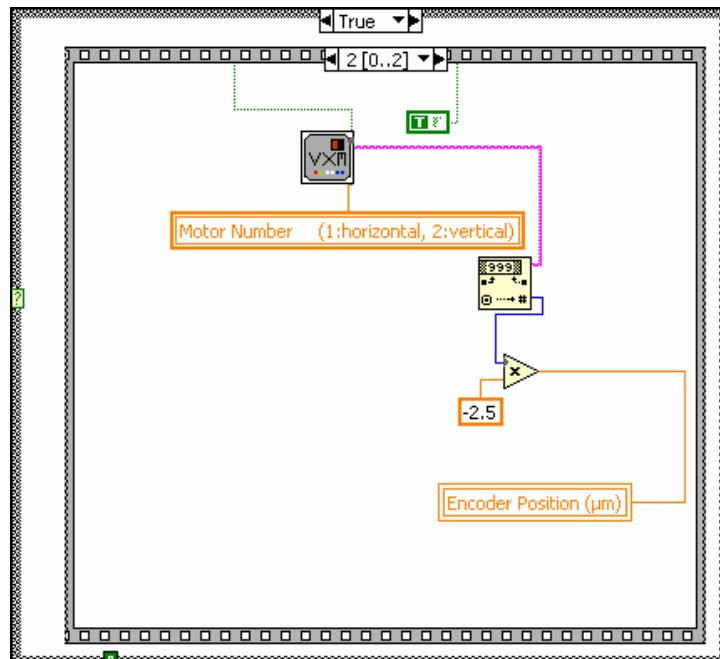


Figure B-6  
Sequence 4,2



*Figure B-7*  
Sequence 4,3



*Figure B-8*  
Sequence 4,4



## **Sequence 5**

In sequence 5, consecutive conditions are checked and executions are decided.

### **5.1.**

The current density value is always larger than start limit value from this point onward. The programmed depth is compared with motor position value. If true, depth is reached and 7 sequences are executed.

#### **5.1.1.**

This step is illustrated in *Figure B-9*. Programmed depth value is taken from primary user inputs section. Current reading is recorded out of Fluke 45 ammeter driver and is converted to current density by dividing the constant electrode tool frontal surface area. Programmed depth is compared with current position value coming from the step count. If the depth is reached, true condition is met, the sequence start from zero. The tool electrode is pulled all the way back by 4000 steps equating 10mm.

Current density values and position data is recorded and saved as a text file for every step and takes place on the rightmost side of the screen. The data is saved to a user defined file at the front panel.

#### **5.1.2-7.**

The consecutive steps are for program termination and position recording. This sequence is followed and same everywhere else when the program needs to be terminated.

The standard consecutive sequences to terminate a program is:

- The program is first executed with an R command.

- Character wait symbol (^) is sent to finish the execution.
- Position data is recorded in buffer for next sequence.
- Online mode is terminated.
- Characters are cleared from the port by sending a true constant to the driver port.
- True constant is sent to terminate the case structure and move to next sequence.

These six standard steps are illustrated in the block diagrams in *Figure B-10* through *Figure B-15*. Remaining of the block diagram is omitted for the sake of simplicity. These six steps will be referred as program termination routines from now on.

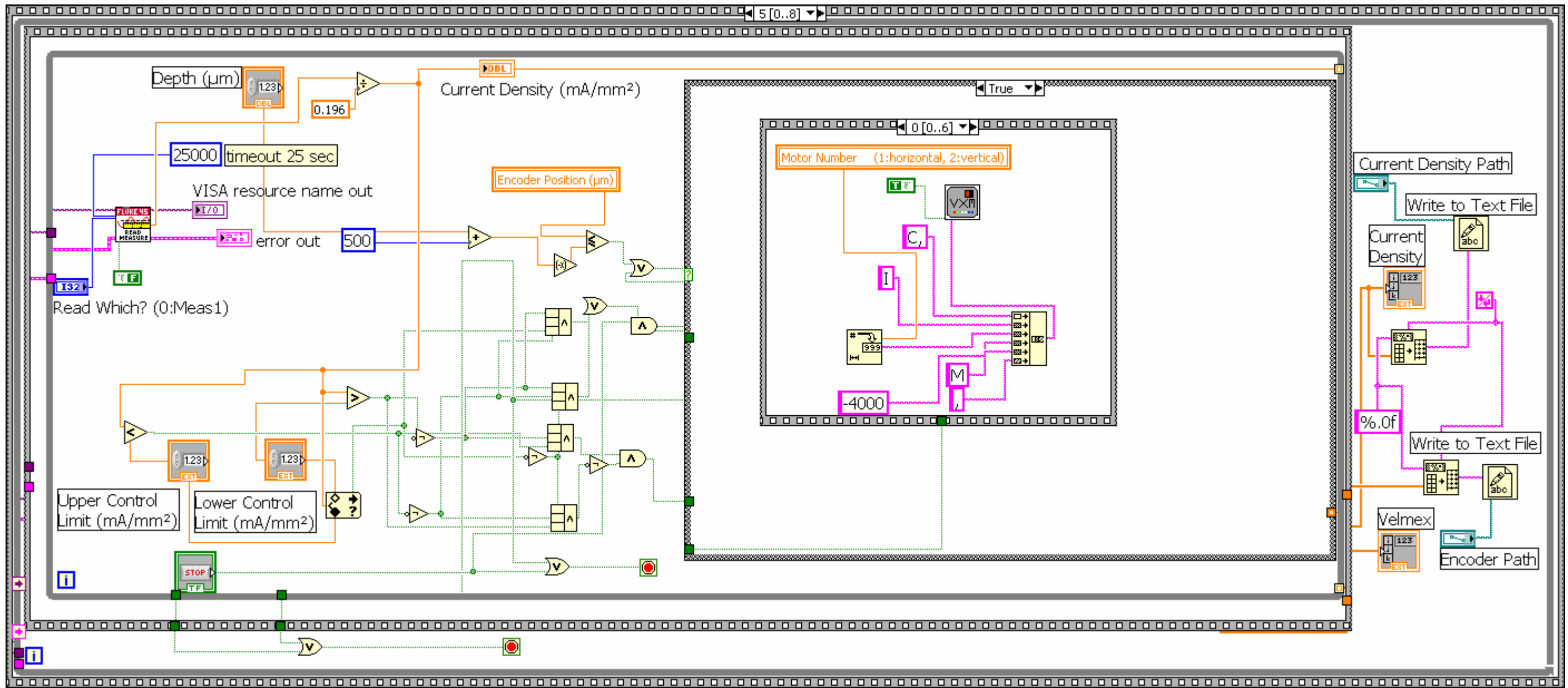


Figure B-9  
Sequence 5,1,1

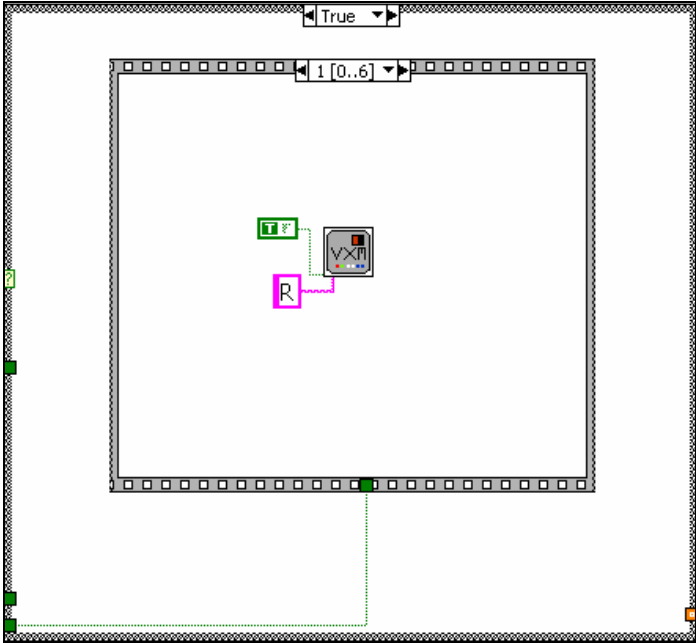


Figure B-10  
Sequence 5,1,2

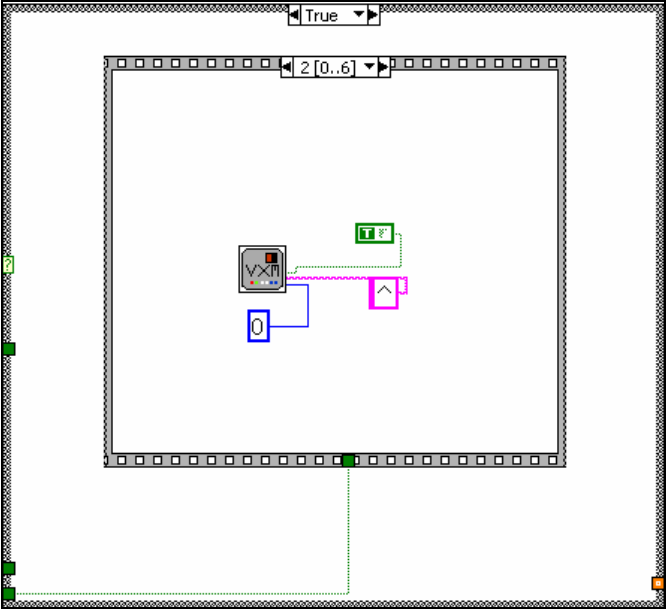


Figure B-11  
Sequence 5,1,3

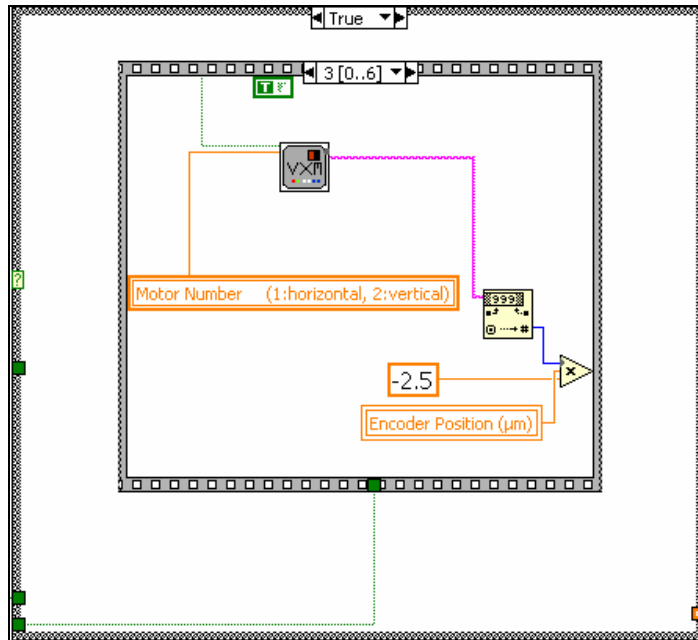


Figure B-12  
Sequence 5,1,4

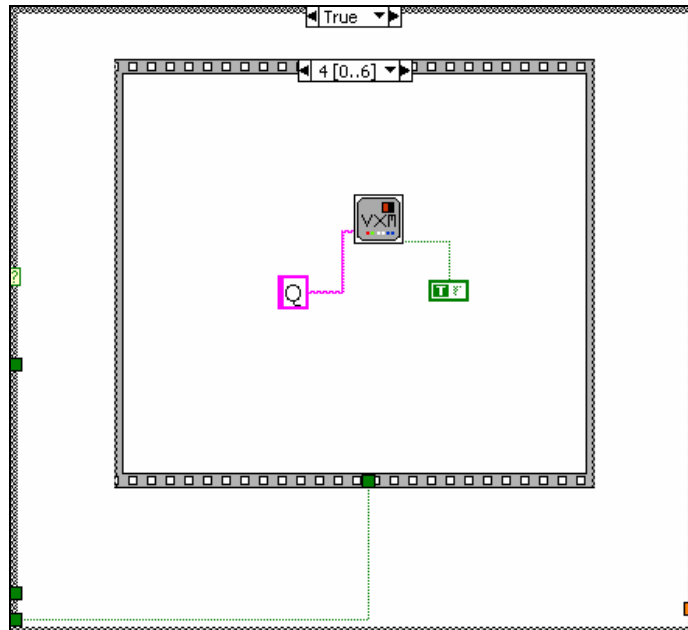


Figure B-13  
Sequence 5,1,5

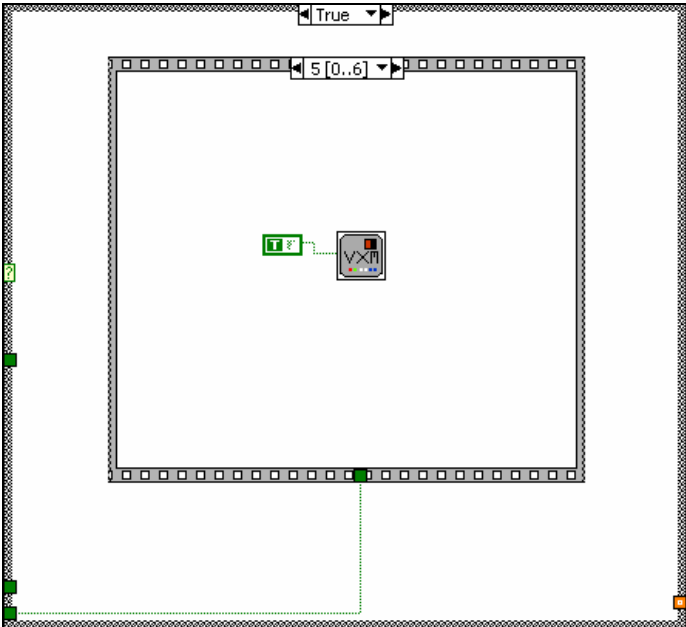


Figure B-14  
Sequence 5,1,6

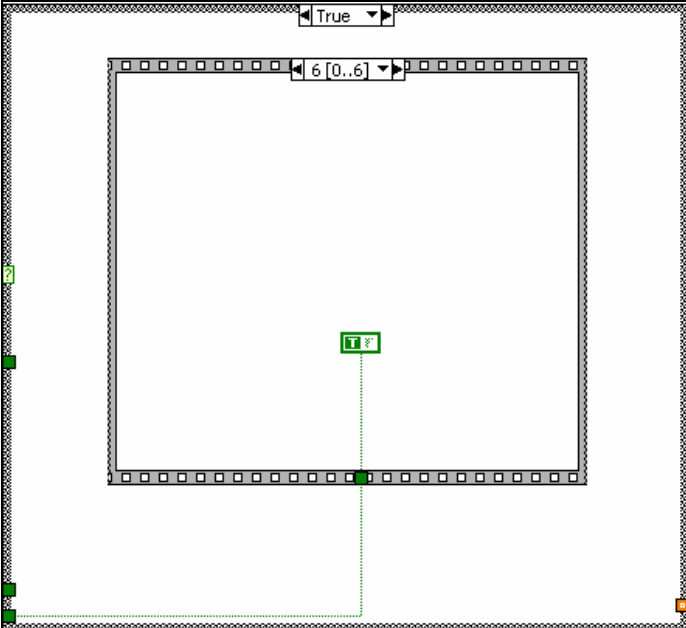


Figure B-15  
Sequence 5,1,7

## 5.2.

In this sequence, false condition is met for the previous comparison. This means the depth is not reached and program executes next sequence.

### 5.2.1.

Another true/false condition check is executed. This time stop button is checked whether it is pressed or not. If pressed, statement goes true. The motor position is recorded one final time and the sequence 5 is terminated. This is shown in *Figure B-16*. Then sequences 6, 7 and 8 are executed. These are most general termination sequences and no other calculation is done anymore.

At sequence 6, wait character symbol is sent and block diagram is same with *Figure B-11*. At sequence 7, online mode is terminated and the block diagram is the same with *Figure B-13*. Finally sequence 8 is when the true constant is sent to driver port to clear the characters and reset for next execution. The block diagram is identical to *Figure B-14*.

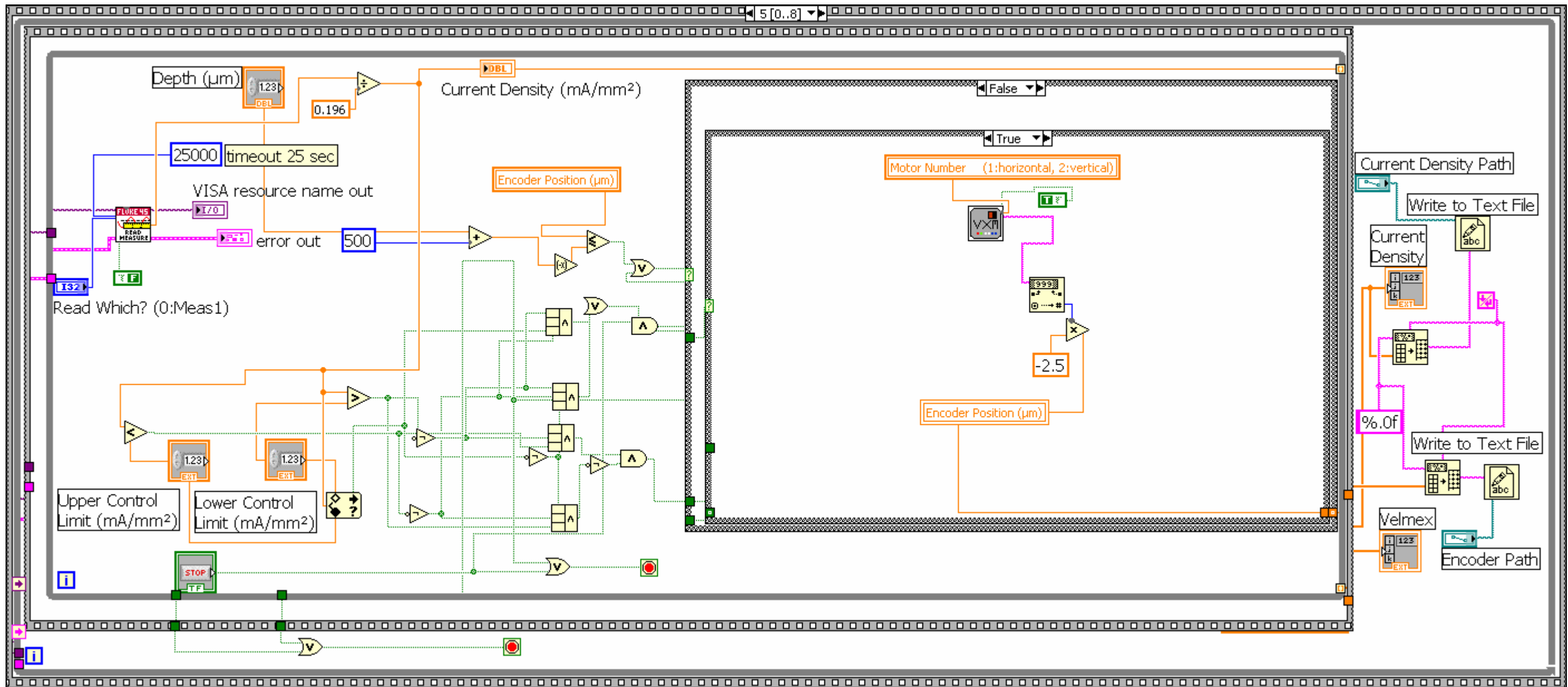


Figure B-16  
Sequence 5,2,1



### 5.2.2.

The stop button press statement goes false if it is not pressed. In this case, yet another true/false sub condition is executed. This time, upper and lower control limits are checked.

If false, the recorded current density value is higher than user set upper value, meaning there is either a short circuit or the tool is very close proximity to workpiece. If that is the case, the tool is pulled back up 4000 steps and program terminated. The pull up sequence is shown in *Figure B-17*. After this execution, program termination is followed by termination routines previously illustrated in *Figure B-10* through *Figure B-15*.

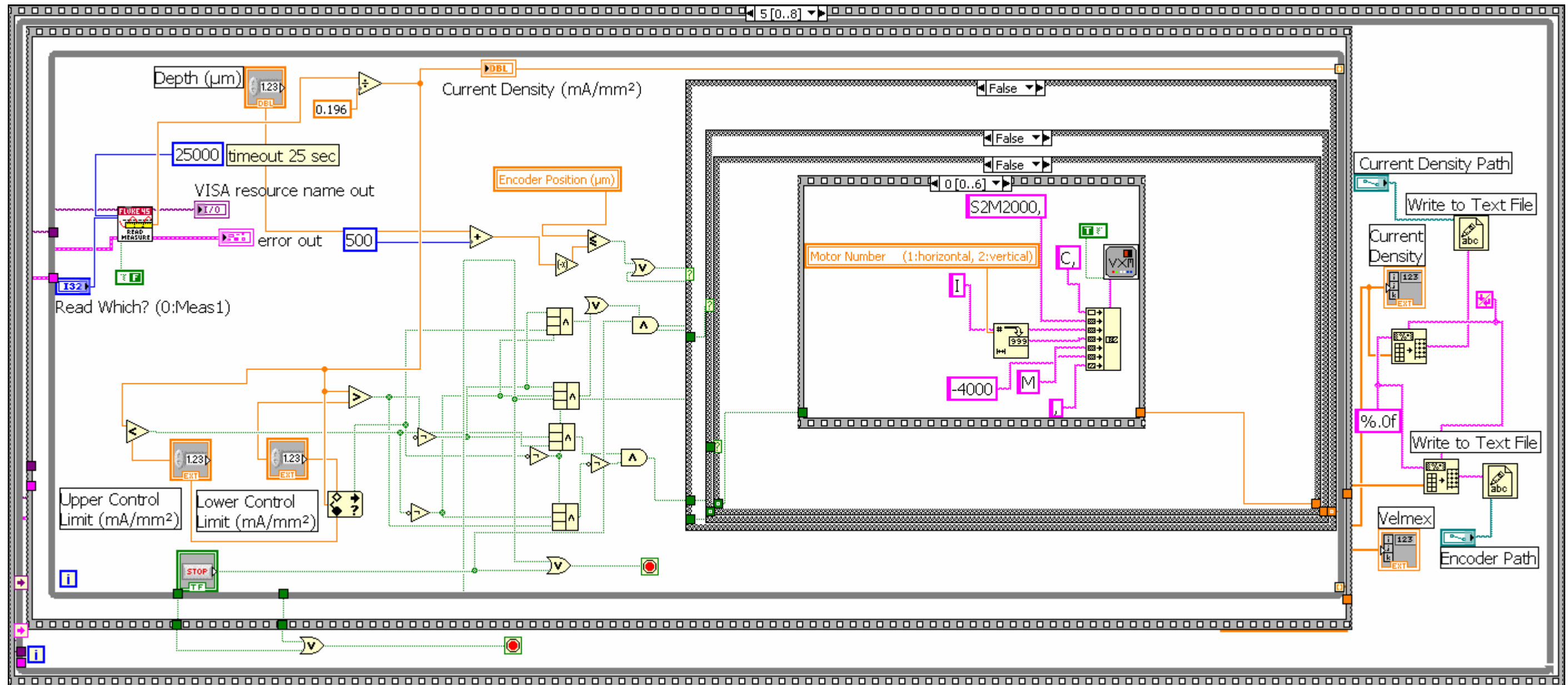


Figure B-17  
Sequence 5,2,2

### 5.2.3.

The condition becomes through if the current density is lower than lower set limit and higher than start set limit. In this particular case, the tool is advanced on the workpiece in user defined steps until the condition is disrupted. This condition is illustrated in *Figure B-18*. Remaining 4 sequences in this sun condition are, running the program, wait character sending, recording the position value and a user defined step wait time. This is the time spent before the next cycle and has a direct effect to actuation speed. Since, step wait is the only new sequence, it is depicted in *Figure B-19*.

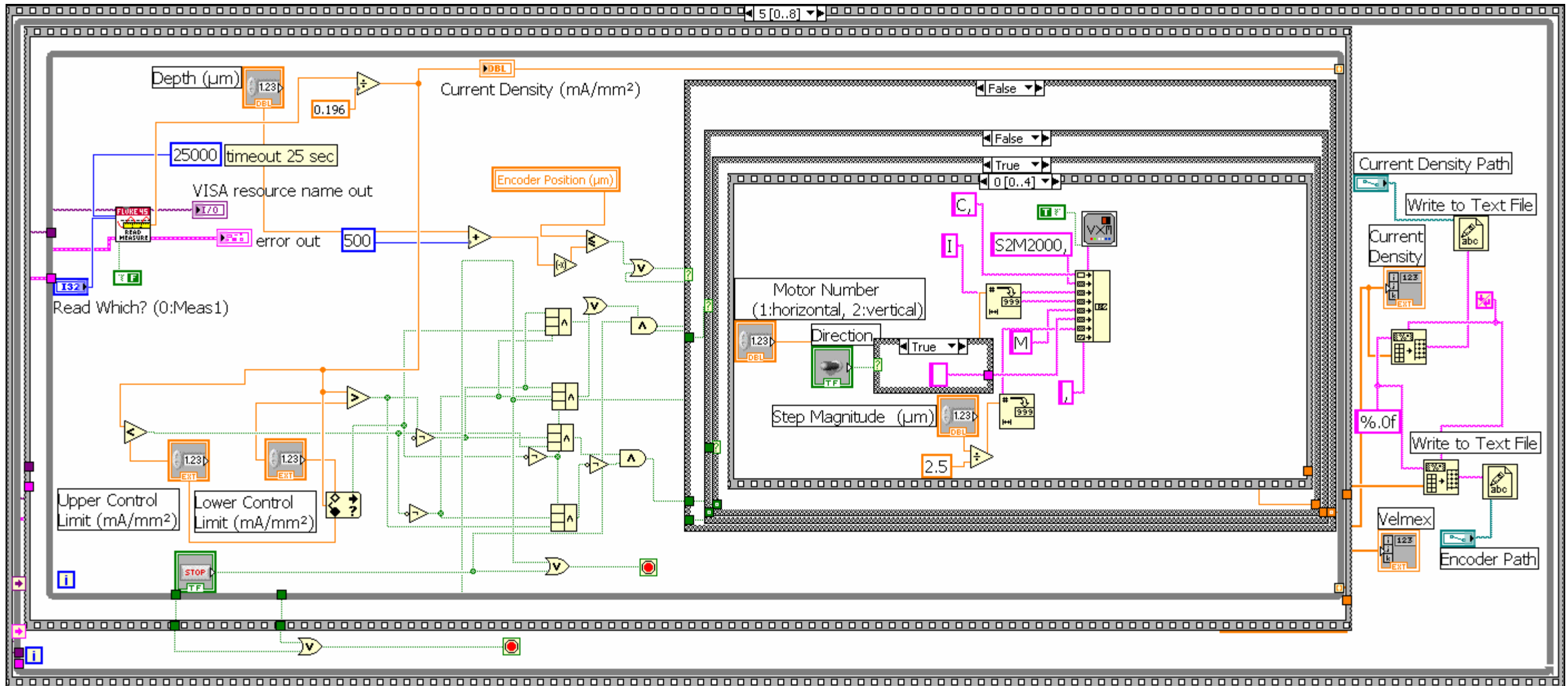
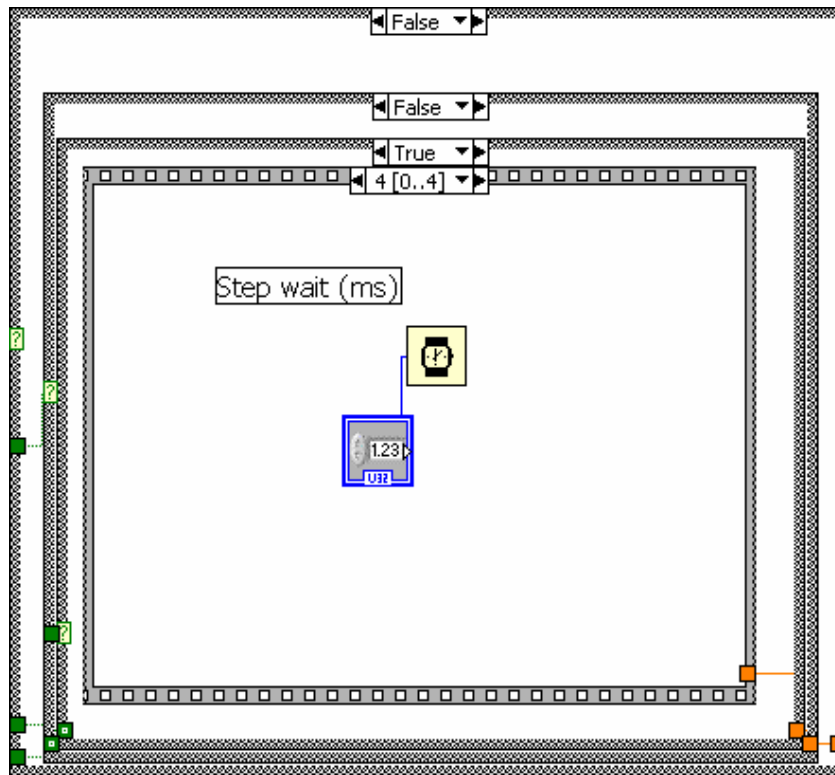


Figure B-18  
Sequence 5,2,3



*Figure B-19*  
**Sequence 5,2,3 termination**

### **Stand-by Condition**

If none of the conditions are met, the only state that is satisfied is when the current density is higher than lower set value and lower than upper set value. In this particular case, the system stands-by, waits until current density drops below the lower set value with material removed and executes previous sequence again. If the stop button is pressed any time while machining, the upper condition loop is satisfied and the machining stops with tool electrode pulled up no matter what the current density value is.

## APPENDIX C

### SERIAL INTERFACE CONNECTIONS

Serial interface connections on PCI-8432/4 board are shown in *Figure C-1*.

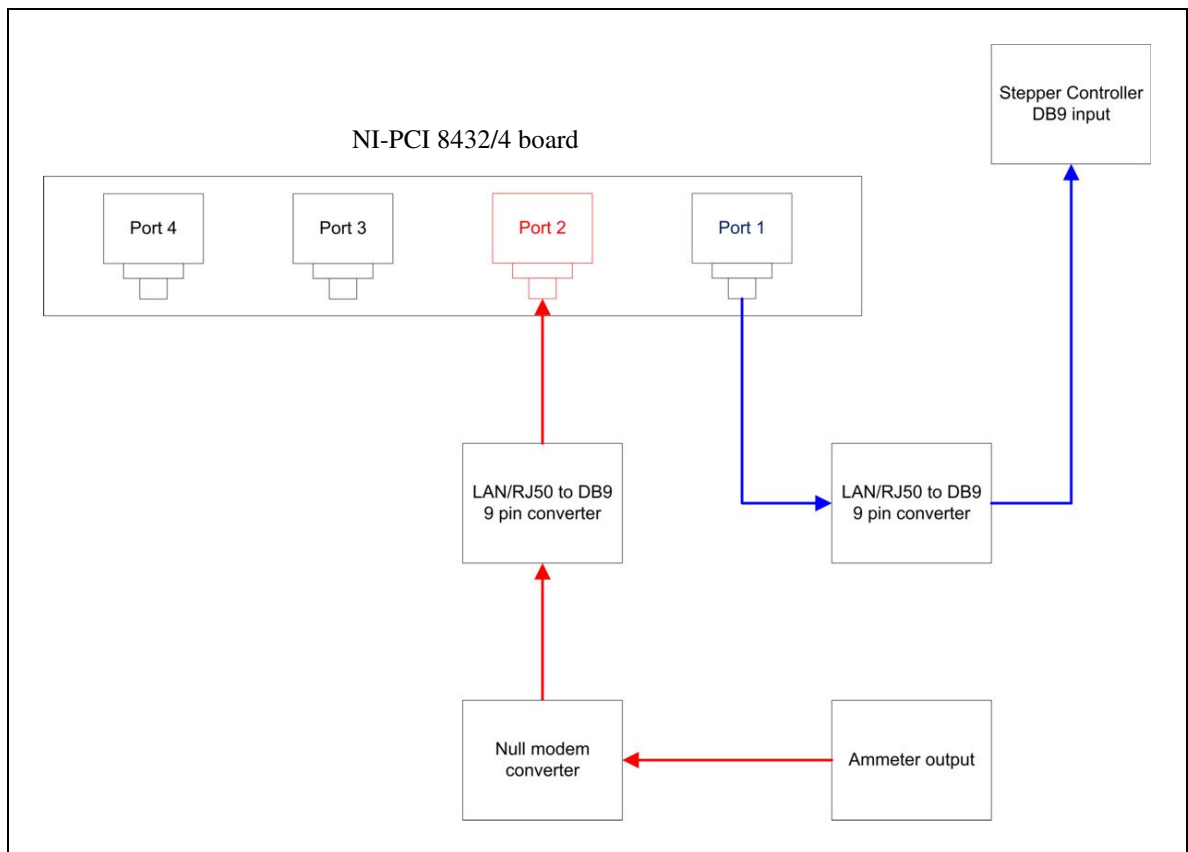


*Figure C-1*  
**Serial interface connections**

## VITA

Fatih Mert Ozkeskin received his Bachelor of Science degree in mechatronics engineering from Sabanci University, Istanbul, Turkey. He began his graduate education in mechanical engineering at Texas A&M University in September 2006 and received his Master of Science degree in August 2008. His research interests include micro/nano manufacturing, MEMS, control systems and robotic applications.

Mr. Ozkeskin can be reached at 65 Ada, Mimoza 3/8, d:17, Atasehir, Istanbul, 34758 TURKEY. His e-mail address is mertozkeskin@gmail.com.